Eigenvector Centrality of the Visual Network exceeds the Default Mode Network during Rest

Franziska Goltz

Donders Institute for Brain, Cognition and Behavior

Faculty of Social Sciences

Radboud University, Nijmegen, the Netherlands

SOW-DGCN05-2019-JAAR-V: Practical Training and Thesis

Department of Biological and Medical Psychology

University of Bergen, Bergen, Norway

Supervisors: Dr. Stavros Skouras, Prof. Dr. Stefan Kölsch

Educational supervisor: Dr. Koen Haak

June 25, 2020

Abstract

The default mode network (DMN) is one of the resting state networks (RSNs) in the brain that have been identified by investigating temporal correlations of spontaneous activity fluctuations in resting state fMRI (rsfMRI). The DMN is crucial for efficient cognitive functioning, although evidently decreasing in activity during many cognitive tasks. Even though the DMN is typically identified by independent component analysis (ICA), other methods have been used to extract and analyze the network as well and their relation to ICA has been explored. However, no comparison of ICA and eigenvector centrality mapping, another data-driven, but graph-theory based method has been reported yet. Here, we used 100 rsfMRI data sets to show that the medial visual network, rather than the DMN, was the most central network during rest and that its eigenvector centrality correlated negatively with the centrality of the DMN. Accordingly, the most central areas during rest did not conform with the DMN extracted by ICA. Our results suggest that the visual RSNs play a more versatile and not strictly modular function during rest and that the investigation of their individual variations is more important than previously believed.

Neuroscientific literature on the default mode network (DMN) has evolved and expanded considerably within the past 20 years (Raichle et al., 2001; Raichle, 2015). The DMN is comprised of the ventral and dorsal medial prefrontal cortex (v/d MPFC), precuneus/posterior cingulate cortex (PCC), retrosplenial cortex, inferior parietal lobe, and lateral temporal cortex – areas, which were shown to decrease activation in response to goal-directed tasks (Shulman et al., 1997) and which were therefore assumed to correspond to a baseline of neural activity in the brain (Raichle et al., 2001). The DMN particularly appears to contribute to internally focused processes such as theory of mind, self-referential thought, and autobiographical

memory (see Buckner, Andrews-Hanna, & Schacter, 2008 for a review), while aberrances of its intra- and inter-network connectivity are associated with e.g. depression (Greicius et al., 2007), autism spectrum disorder (Kennedy, Redcay, & Courchesne, 2006), disorders of consciousness (Soddu et al., 2012), attention deficit hyperactivity disorder (ADHD) (Tian et al., 2006), and Alzheimer's disease (AD) (Filippini et al., 2009; Binnewijzend et al., 2012; Hafkemeijer, Grond, & Rombouts, 2012; Broyd et al., 2009; Andrews-Hanna, Smallwood, & Spreng, 2014). Recent studies have further focused on potential roles of the network's subcomponents (e.g. Andrews-Hanna et al., 2010; Kernbach et al., 2018) and more defined activation patterns of its most important hubs, like the PCC (Leech, Kamouriek, Beckmann, & Sharp, 2011).

The DMN, along with other resting state networks (RSNs), is typically identified by the investigation of temporal correlations of activity fluctuations in resting state fMRI (i.e. resting state functional connectivity) and the ensuing extraction of coherent connectivity patterns with e.g. seed based connectivity analysis (SCA) (Biswal et al., 1995; Fox et al., 2005) or independent component analysis (ICA) (Comon, 1994; McKeown et al., 1998; Pruim et al., 2015). In SCA, the functional relationship between a region of interest (ROI) and the remaining brain is defined by correlating its timeseries to the timeseries of every other voxel. In contrast, ICA is a multivariate and explorative approach, in which the data is decomposed into a number of statistically independent components by maximizing the negative entropy and thereby optimizing non-Gaussianity in the data (Hyvärinen & Oja, 1997; Beckmann & Smith, 2004; Beckmann, DeLuca, Devlin, & Smith, 2005). Recently, ICA has gained significant importance in network modelling (e.g. Zuo et al., 2010; van den Heuvel, Mandl, Kahn, & Hulshoff Pol, 2009; Damoiseaux et al., 2006; see Beckmann, 2012 for an overview), as it is able to identify coherent connectivity patterns without an *a priori* hypothesis about their spatial or temporal layout.

Along with the prominent application of ICA for functional connectivity analyses, its relation to other methods has been explored. For example, several studies compared the sensitivity of ICA and SCA with regard to age related changes in DMN connectivity (Koch et al., 2010; Bluhm et al., 2008). Results showed that reductions of co-activation magnitude in the DMN could only be detected with ICA. Also, evidence suggests that ICA has lower diagnostical power compared to volume of interest analysis regarding the classification of AD patients and healthy controls (Koch et al., 2012). Nevertheless, overall, ICA, SCA, and regional homogeneity analysis have been shown to derive a concordant spatial map of the DMN and task-positive network in healthy participants (see e.g. Long et al., 2008 for a direct comparison). Therefore, advantages and disadvantages of the respective methods have been further discussed (Cole, Smith, & Beckmann, 2010; Li et al., 2009). It has been emphasized that SCA is particularly sensitive to confounds like structural noise and RSNs that are not of interest, and that its interpretation is restricted to and biased by the selected ROIs. In contrast, ICA appears to account better for noise and avoids prior assumptions of ROIs. Yet, the iterative nature of the decomposition leads to variability across runs (e.g. multiple runs of ICA on the same dataset) and there is no ideal model order selection possible based on neurophysiology. Consequently, the number of extracted components is somewhat arbitrary and their interpretation and classification can be difficult, specifically in high order decompositions (Cole et al., 2010; Li et al., 2009).

A method that addresses the challenges of both SCA and ICA is eigenvector centrality mapping (ECM). ECM is completely data-driven and operates without any *a priori* defined parameters, such as specifying the dimensionality in ICA, or ROIs in SCA. Beyond that, ECM considers the interregional connectivity of the *entire* brain, rather than parcellating the brain into distinct networks, or only considering specific ROIs. ECM is a graph-theory based method (Lohmann et al., 2010; Bonacich, 1972) which has recently been introduced and applied to fMRI data in the context of AD and its biomarkers (Binnewijzend et al., 2014;

Skouras et al., 2019; Skouras et al., 2020), DMN connectivity (Taruffi, Pehrs, Skouras, & Koelsch, 2017), attentive object tracking (Alnæs et al., 2015), emotional network modeling (Koelsch & Skouras, 2014), and others (Hadriche, Jmail, Blanc, & Pezard, 2019; Hove et al., 2015; Markett et al., 2015; Wink et al., 2012). The method derives a 3D spatial map of the most influential areas in the brain by identifying voxels that are most connected to other voxels that are themselves highly central. The eigenvector centrality of a voxel is thus not only determined by the degree of the voxel (meaning the number of voxels each voxel is connected to), but also by the importance of each respective connection, thereby considering the entire network hierarchy. Theoretically, this is achieved by 1) determining a correlation matrix of the time series of all possible voxel pairs, 2) defining each voxels' first order centrality measure by the sum of the correlation coefficients of all its connections (i.e. degree centrality), 3) iteratively updating the centrality measure of each voxel with the sum of all its connections, but weighted by each connections' centrality measure from the previous iteration. Eventually, with a proportionality factor of $1/\lambda$, where λ is the largest eigenvalue of the similarity matrix, this process would converge to an eigenvector of the biggest eigenvalue of that matrix. The *i*-th entry of the eigenvector then describes the eigenvector centrality of the *i*-th voxel. In ECM, the respective eigenvector is determined by the power iteration method (Golub & Loan, 1996; see Lohmann et al., 2010 for further mathematical details about ECM). Like other centrality measures, eigenvector centrality has been evidenced to be valuable in identifying networks and their most influential nodes in a parsimonious manner (Joyce, Laurienti, Burdette, & Hayasaka, 2010; Zuo et al., 2012; Bullmore & Sporns, 2009). Thus, similar to ICA, ECM is a state-of-the-art voxel-wise and data driven connectivity analysis method. Yet, to our knowledge, up to date no systematic comparison has been reported between the two.

In the present study, we investigate how ICA and ECM relate to and complement each other when it comes to the interpretation of functional connectivity during resting state, with

particular focus on the DMN. We explore whether the most central regions during rest, as indicated by their eigenvector centrality (EC), overlap with the regions that are to date considered to constitute the DMN. In other words, we ask the question: To what extent are the core areas of the temporally most coherent task-negative network also the most influential areas during resting state? To answer this question, we use 100 independent resting state fMRI (rsfMRI) datasets from the 'Human Connectome Project 1200 Subject release' (van Essen et al., 2013) and we compare the DMN, derived by probabilistic ICA, to the most influential areas during rest, derived by ECM. Importantly, different results are premised on the computational bases for the two methods[1]. Yet, with this study, we want to specifically establish the differences in the main clusters and show how both methods can complement each other with regard to the interpretation of functional connectivity during rest. Previous studies investigating the brain's network structure with a variety of methods have consistently reported the precuneus/PCC, MPFC, inferior parietal lobe, and lateral temporal cortex as intrinsic connectivity hubs during rest (e.g. Yeo et al. (2011) and Lee et al. (2012) using clustering algorithms; Tomasi and Volkow (2011a), Power et al. (2011), and Sporns (2013) using graph-theory; Smith et al. (2009) using ICA on task- and resting state fMRI; Long et al. (2008) using SCA, ICA and ReHo; Andrews-Hanna et al. (2010) using correlation- and cluster based analysis). Therefore, we expected to find high EC in those areas as well. Secondly, we expected that areas comprising the DMN, rather than other RSNs, would show the highest EC during rest.

Methods

Dataset

[1]Probabilistic ICA (PICA) assumes that the data, a p x n matrix with p = time points and n = voxels, is composed of multiple independent spatial components and their timeseries plus noise. To decompose that data, an unmixing matrix is approximated and optimized in a way that derives maximally independent components (Hyvärinen & Oja, 1997; Beckmann & Smith, 2004). In contrast, ECM (Lohmann et al., 2010) operates by approximating the principal eigenvector of the data's similarity matrix. This is similar to principal component analysis, which approximates *orthogonal* components. Thus, while ICA is based on statistical independence, ECM is based on orthogonality (McKeown et al., 1998).

In this study, rsfMRI data of the WU-Minn Human Connectome Project (HCP) 1200 Subject release was used (https://www.humanconnectome.org; van Essen et al., 2013). Specifically, 100 unrelated, healthy subjects (M_{age} = 29.41, SD_{age} = 3.56, 54 females and 46 males) were assessed to provide independent measures and evade controlling for the HCP family structure. Under the HCP protocol, all subjects gave written consent and data acquisition was approved by the institutional review board of Washington University, St. Louis.

Image acquisition

Acquisition methods of anatomical and functional images are described in detail elsewhere (van Essen et al., 2012; van Essen et al., 2013; Glasser et al., 2013). T1 weighted anatomical, as well as functional MR images were acquired on a customized Siemens 3T Connectome Skyra scanner using a 32-channel head coil. A 3D MPRAGE T1-weighted sequence (TR = 2400ms, TE = 2.14ms, TI = 1000ms, FA = 8°, field of view (FOV) = 224x224mm, bandwidth = 210Hz/Px) was used to acquire structural images with a 0.7mm isotropic resolution. Multiband multislice gradient-echo echo planar imaging (GE-EPI; Moeller et al., 2010; Xu et al., 2012) was used for blood oxygen dependent (BOLD) contrast based functional acquisitions (TR = 720ms, TE = 33.1ms, FA = 52°, slice thickness = 2mm, 72 slices, 2mm isotropic resolution, multiband factor = 8, time points = 1200, bandwidth = 2290Hz/Px) and phase encoding was applied in left-right/right-left (L-R/R-L) direction using an asymmetric acquisition matrix (104x90) with a 208x180mm FOV. A total of one hour resting state acquisition was split into two imaging sessions, with two 15-minute runs each. In every session, one run was acquired with L-R phase encoding, one with R-L, the order of which was counterbalanced. During resting state data acquisition, participants kept their eyes open, relaxed and fixated on a bright fixation cross superimposed over a dark background. They were instructed to stay awake, look at the fixation cross, and think of nothing in particular.

Preprocessing

Images in volumetric space had been preprocessed by the HCP minimal preprocessing and ICA-FIX pipeline (for full details see Glasser et al., 2013 and Smith et al., 2013). Briefly, these pipelines were built using tools of the FMRIB Software Library (FSL; Jenkinson et al., 2012), FreeSurfer (Fischl, 2012), and Connectome Workbench (Marcus et al., 2013). The functional data of every participant underwent correction for gradient distortion, subject motion, as well as EPI distortion, registration to the subject's high-resolution T1-weighted structural image and MNI-152 standard space. All correction and registration transforms were combined into one nonlinear transformation for a single spline interpolation. All images were brain masked and their 4D whole brain mean intensity was normalized to 10,000. Temporal preprocessing included a high pass filter (2000s cut-off) and every 15-minute run was denoised using the FIX method (FMRIB's ICA-based X-noisifier; Smith et al., 2013). Additionally, all images were smoothed by a Gaussian kernel of 6mm full width at half maximum (FWHM) and resampled to 3mm isotropic resolution.

Independent component analysis

Spatial group-ICA was carried out on the concatenated timeseries data of 100 subjects (four runs each) by means of PICA (Beckmann & Smith, 2004), which is implemented in FSL's MELODIC (Multivariate Exploratory Linear Optimized Decomposition, version 3.15; www.fmrib.ox.ac.uk/fsl). Inherent preprocessing included masking of non-brain voxels, temporal demeaning, variance normalization, and data reduction using principal component analysis. The dimensionality was set to 20 (d = 20), based on previous literature indicating that 20-25 components reliably show the most anatomically relevant RSNs (e.g. Smith et al., 2009; Damoiseaux et al., 2006; Laird et al., 2011). Raw IC maps were transformed to Z-maps based on the estimated voxel-wise standard deviation of the noise. Finally, spatial maps were thresholded with alternative hypothesis testing by fitting a Gaussian/gamma mixture model to the voxel intensity distribution of the spatial maps with a threshold of $P > 0.5$ (Beckmann et

al., 2005; Hartvig & Jensen, 2000). Given the loss function associated with the estimation process, this threshold assigns equal concern to false-positives and false-negatives (Hartvig & Jensen, 2000). Voxels surviving this thresholding had a modelled relative probability of being 'active' that was higher than their probability of being 'noise'. Spatial cross correlation ($P < .005$, corrected for multiple pairings) of all components against previously defined RSNs (Smith et al., 2009) was used to define nine RSNs of interest, including the default mode, medial visual, lateral visual, auditory, left and right frontoparietal, sensory motor, occipital pole, and executive control network.

Eigenvector centrality mapping

ECM as described in Lohmann et al. (2010) was applied to all subjects' preprocessed whole-brain data using LIPSIA v3.1.0 (released May 13, 2019; Lohmann et al., 2001). Eigenvector centrality measures were derived by approximating the principal eigenvector of the temporal correlation matrix of every dataset, using the power iteration method (Golub & Loan, 1996). The EC of each voxel then corresponded to the weighted sum of ECs of that voxel's direct neighbors, scaled by a proportionality factor of $1/\lambda$. To maximize interpretability and comparability with our previous ECM studies (Koelsch & Skouras, 2014; Taruffi et al., 2017; Koelsch, Skouras, & Lohmann, 2016; Skouras et al., 2019; Skouras et al., 2020), EC values were based on positive correlations, meaning that negative correlations in the correlation matrix (also known as beta-centrality) were set to zero (see Skouras et al., 2019 for a detailed justification). This analysis resulted in four EC maps per subject, one map for every dataset (coming from two acquisition sessions with two runs in each session).

Statistical Inference

To ensure that centrality measures were comparable across runs and subjects, every EC map was standardized to an ECz-map, with $ECz_i = (EC_i - \mu)/\sigma$, $1 \leq i \leq N$, where μ and σ are mean and standard deviation of the EC across all N voxels in the brain (Zuo et al., 2012; Buckner et al., 2009). The respective four ECz-maps were averaged per subject, resulting in

100 standardized EC maps. To identify voxels with significant EC in the brain, a nonparametric one-sample t-test was performed on the 100 ECz-maps using FSL *randomise* (1,000,000 permutations). Multiple comparisons were FWE corrected using TFCE (threshold free cluster enhancement; Smith & Nichols, 2009) and thresholded at $P_{corrected} < .000005$. To investigate and compare EC values across RSNs, every subject's weighted average ECz was computed for each relevant component (i.e. default mode, medial visual, lateral visual, auditory, left and right frontoparietal, sensory motor, occipital pole, and salience/executive control network) using FSL (*fslmeants* routine). Then, the computed network-specific ECz's were entered as the dependent variable in a repeated measures MANOVA with RSN as the within subjects factor[2].

Results

Independent component analysis

Nine independent components corresponding to the most consistently reported RSNs (Beckmann et al., 2005; Smith et al., 2009; Laird et al., 2011; Cole et al., 2010) were identified by means of spatial cross-correlation to the 10 components reported by Smith et al. (2009) (mean $r = .59$ (0.31; 0.77), $P_{corrected} < .005$). None of the components in the present study correlated significantly with the component comprising only the cerebellum ("RSN 5" from Smith et al., 2009). As there were no explicit hypotheses about the connectivity of that area, we did not further consider the cerebellum as an RSN. Accordingly, the following nine networks were assessed from the data (reported in the order of variance explained by the respective component; see Figure 1 and Appendix, Figure A1):

(1) *Default mode*: This component comprised the ventral precuneus, PCC, MPFC, superior frontal gyrus, and middle, superior temporal lobe. Furthermore, the angular

[2]A repeated measures ANOVA assumes sphericity, i.e. equal variance of the differences between within-subject pairs. In cases where that assumption is violated, a repeated measures MANOVA, which uses difference scores as dependent variable, has higher power than available corrections for a repeated measures ANOVA, if the sample size is relatively large ($N \geq K+30$, where K = number of conditions) and epsilon is low (< .85) (O'Brien & Kaiser, 1985; Algina & Keselman, 1997). Both methods are implemented in SPSS (IBM Statistical Package for Social Sciences; version 25). Here, given the strong violation of sphericity (indicated by Huyn-Feldt epsilon = 0.334) and a large sample, a MANOVA was conducted.

gyrus, hippocampus, and parts of the cerebellum (including Crus I and Crus II) belonged to this component.

(2) *Medial Visual*: The medial visual component comprised primary visual areas, including the intra calcarine cortex and superior occipital gyrus, the cuneus, and lingual gyrus.

Figure 1

ICA results

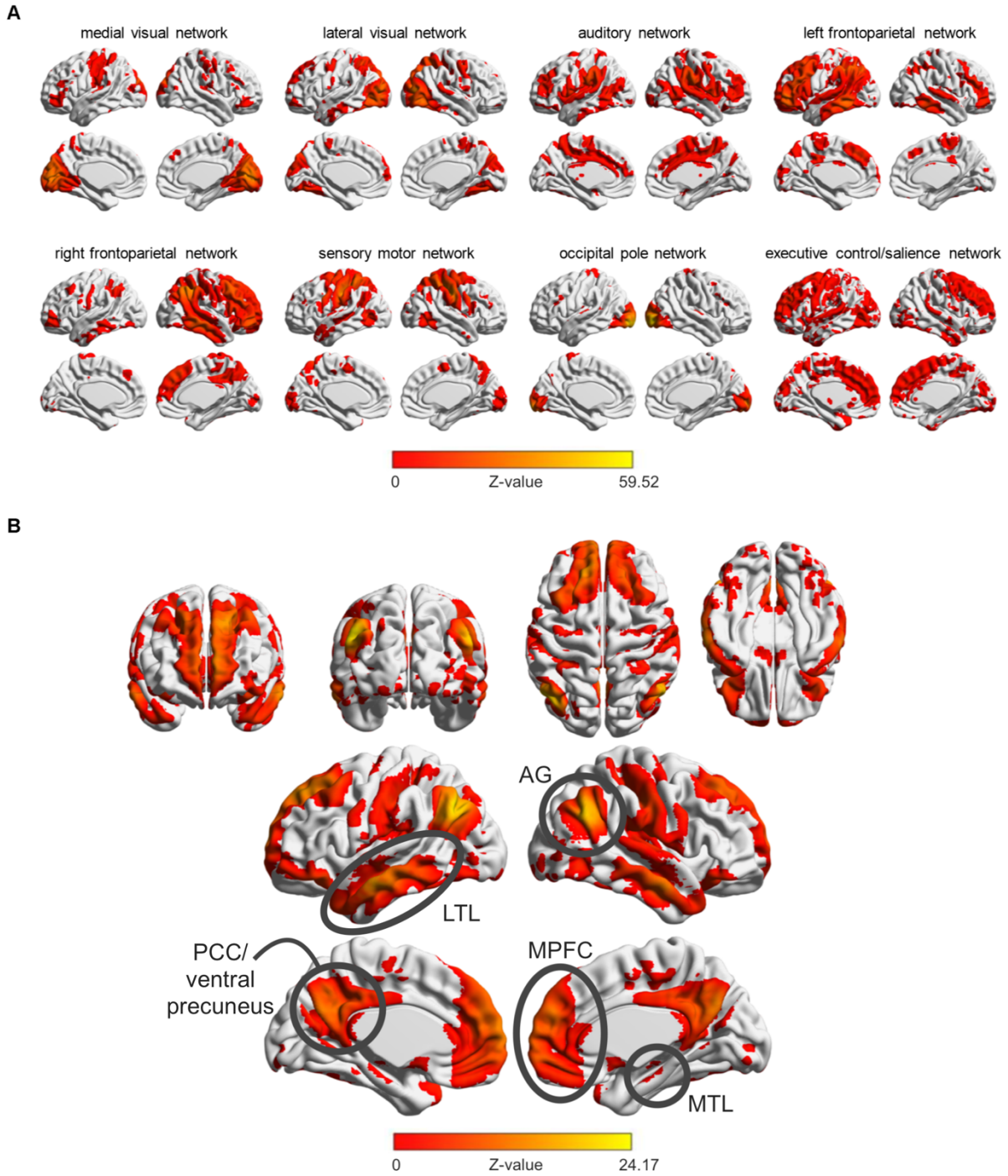

Note. **A.** Left and right lateral (top) and medial (bottom) views of thresholded Z-maps of eight independent components estimated by probabilistic group ICA (d = 20) of 100 healthy subjects. Thresholded by fitting a Gaussian/gamma mixture model to the data, with P > 0.5. Positive Z-values were mapped on an ICBM152 brain surface. **B.** Full view of the thresholded DMN. Top row shows anterior, posterior, dorsal, and ventral view, middle and bottom row show left and right lateral and medial views, respectively. Positive Z-values were mapped on an ICBM152 brain surface. AG = angular gyrus, LTL = lateral temporal lobe, PCC = posterior cingulate cortex, MPFC = medial prefrontal cortex, MTL = medial temporal lobe.

(3) *Lateral Visual*: This component mainly comprised extrastriate visual areas in the lateral

occipital cortex, including the middle and inferior occipital gyrus.

(4) *Auditory*: The auditory component comprised areas in the primary and secondary auditory cortices, among which the temporal pole, planum temporale and planum polare, Heschl's gyrus, and anterior supramarginal gyrus. The anterior cingulate was also part of this network.

(5) *Frontoparietal left lateralized*: This component spanned frontal and parietal areas, including the angular gyrus, inferior frontal gyrus, medial frontal lobe, and superior parietal lobe, as well as parts of the temporal gyrus. Its mirrored counterpart, component (6), which comprised the *frontoparietal right lateralized* network**,** covered homotopic areas in the right hemisphere.

(7) *Sensory Motor*: Above threshold areas in this component were the pre- and postcentral gyrus, supplementary motor area, and anterior supramarginal gyrus.

(8) *Occipital Pole*: This component comprised the occipital pole, i.e. primary visual areas.

(9) *Executive Control*/*Salience*: Here, lateral and medial frontal areas (including middle frontal gyrus, superior frontal lobe), as well as the paracingulate gyrus, temporal pole, and anterior cingulate gyrus were covered.

Eigenvector centrality mapping

The nonparametric one-sample t-test on the standardized EC maps showed that most voxels were significant (FWE corrected $P < .000005$). Further, due to the exceedingly high significance observed, combined with the unfeasible amount of permutations needed for a more precise significance estimate, the range of p-values was limited and the corrected p-values reached a ceiling value (corresponding to $Z = 4.75$). Therefore, the local maxima of the most central areas (mean $ECz > 1.6$) within all significant voxels were identified to enable a meaningful interpretation. These included primary and secondary visual areas in the intra- and supra-calcarine cortex (BA17), the medial occipital cortex, particularly the cuneus (BA18/BA19), as well as the superior lateral occipital lobe (BA19). Also, the supramarginal

gyrus (BA40), the superior parietal lobe/posterior dorsal precuneus (BA7), and postcentral gyrus/parietal operculum (BA1, 2 & 3) were significant and highly central (Table 1, Figure 2).

Table 1

Most central areas with significant EC

Brain region	Brodmann area (BA)	Local max ECz value* M (SD)	MNI-coordinate (x)	MNI-coordinate (y)	MNI-coordinate (z)
Lateral occipital lobe	BA19	2.33 (0.85)	-27	-87	27
Superior parietal lobe/ Precuneus	BA7	2.54 (0.86)	9	-80	45
Calcarine cortex	BA17	1.62 (0.79)	-3	-87	3
Medial occipital lobe/Cuneus	BA18/BA19	1.70 (0.98)	3	-80	27
Inferior parietal lobe/ Supramarginal gyrus	BA40	1.61 (0.91)	57	-30	27
Postcentral gyrus/Parietal operculum	BA1, 2 & 3	2.40 (0.90)	-61	-21	15

*All specified areas had a Z statistic of 4.75, see *Eigenvector Centrality Mapping* section in Results for a more detailed explanation.

Note. ECz values represent mean standardized EC values at respective MNI coordinates, with voxel-wise standard deviation (SD) in parentheses.

Comparison

To investigate which RSN had the highest EC, a repeated measures MANOVA (using the multivariate approach following O'Brien & Kaiser, 1985) with average ECz as dependent variable and RSN (default mode/medial visual/lateral visual/auditory/left frontoparietal/right frontoparietal/sensory motor/occipital pole/executive control) as within subjects factor was conducted (N = 100). With a significant multivariate test (F(8,92) = 273.120, p = 1.28E-60), the univariate contrasts showed that the mean ECz of the DMN was significantly lower than the mean ECz of both the medial and lateral visual network (F(1,99) = 93.707, p = 5.45E-16,

eta^2 = . 486 and $F(1,99)$ = 66.035, p = 1.29E-12, eta^2 = .400, respectively). Also, the mean ECz

Figure 2

ECM results

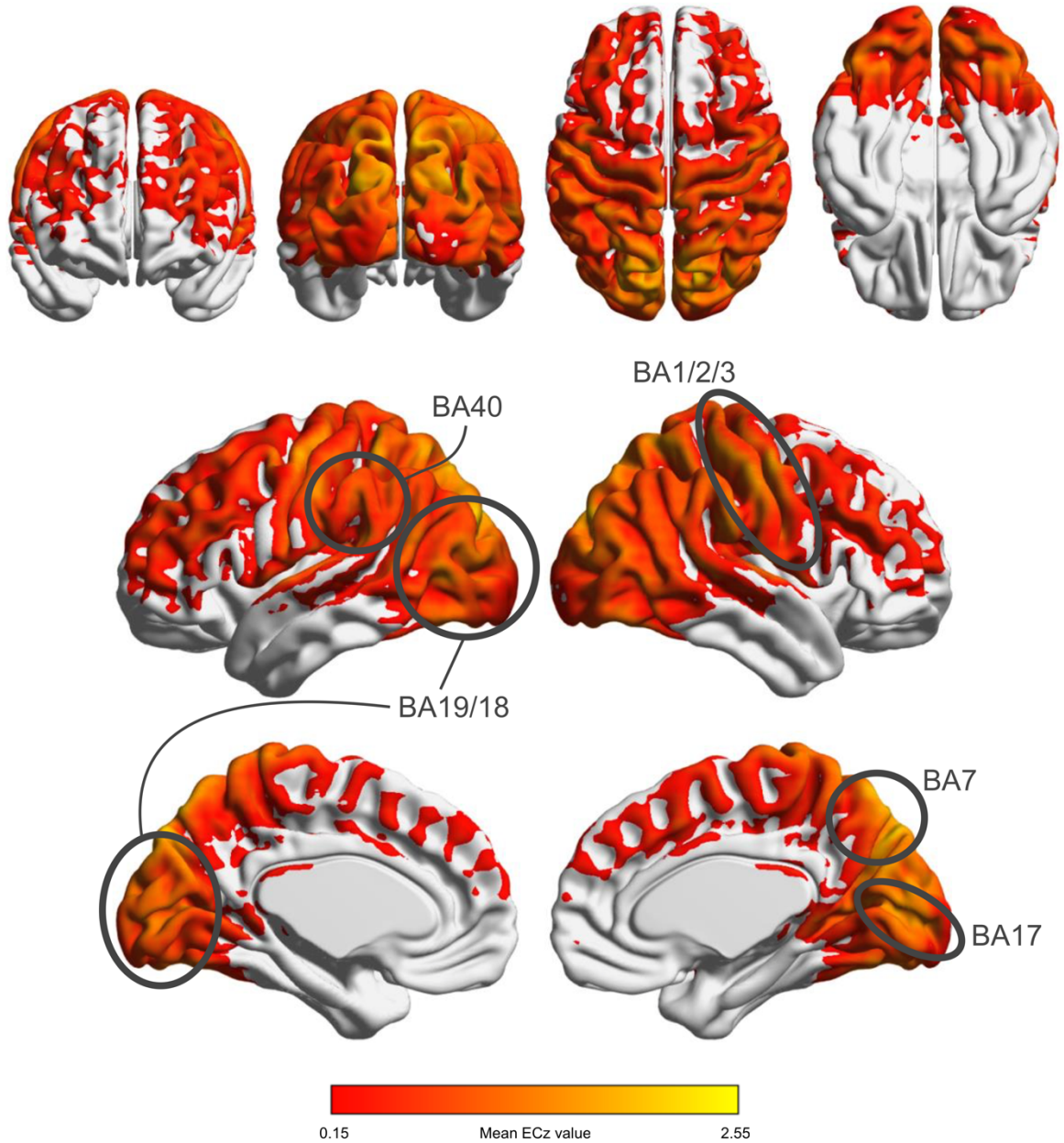

Note. Full view of thresholded ECM results mapped on an ICBM152 brain surface. Top row shows anterior, posterior, dorsal, and ventral view, middle and bottom row show left and right lateral and medial views, respectively. Thresholding was done using TFCE, FWE corrected P < .000005. The most central areas (mean ECz > 1.6) are labelled. BA = Brodmann area.

of the auditory, sensory motor, and occipital pole network was significantly higher than the mean ECz of areas in the DMN ($F(1,99)$ = 67.539, p = 8.16E-13, eta^2 = .406; $F(1,99)$ =

34.315, p = 6.15E-8, eta^2 = .257; $F(1,99)$ = 18.437, p = 4.99E-5, eta^2 = .157 respectively). The mean ECz in the executive control network was significantly lower than the mean ECz of the DMN ($F(1,99)$ = 56.863, p = 2.28E-11, eta^2 = .365). See Table 2 (and Table A1, Appendix) for pairwise comparisons and corrected p-values. To further explore the relation between the centrality of the different networks, Pearson's correlations between the average ECz of all nine RSNs were calculated (Table 3). In line with the results of the MANOVA, it appeared that EC in the medial and lateral visual network correlated negatively with EC in the DMN (r = -.466, p_{corr} = 8.10E-5 and r = -.537, p_{corr} = 6.61E-7; p-values are Bonferroni corrected for multiple comparisons) (Figure 3). In contrast, EC of the frontoparietal networks correlated positively with EC in the DMN (r = .373, p_{corr} = 0.011 and r = .438, p_{corr} = 4.05E-4).

Table 2

Descriptives of nine RSNs

RSN	% of explained variance in ICA	Average Mean ECz	SD ECz	T (df = 99)	$P_{uncorrected}$ against DMN	$P_{corrected}$ against DMN
DMN	6.12	0.3578	0.375	-	-	-
Medial Visual	6.11	1.0020	0.402	9.680	5.45E-16	4.36E-15
Lateral Visual	5.66	0.8003	0.242	8.126	1.29E-12	1.03E-11
Auditory	5.40	0.7756	0.224	8.218	8.16E-13	6.53E-12
Frontoparietal left	4.99	0.3939	0.318	0.924	ns	ns
Frontoparietal right	4.92	0.4437	0.283	2.402	0.018	ns
Sensory Motor	4.91	0.6493	0.202	5.858	6.15E-8	4.92E-7
Occipital Pole	4.33	0.5857	0.349	4.294	4.99E-5	3.99E-4
Executive control	3.63	0.0787	0.135	-7.541	2.28E-11	1.82E-10

Note. Percentage of explained variance was reported per RSN and adopted from ICA MELODIC's output report. Per RSN, the average of mean ECz values and their standard deviation (SD) is stated. The mean ECz of the default mode network (DMN) was compared to the mean ECz of every other RSN, P-values are Bonferroni corrected for multiple comparisons. ns = non-significant.

Discussion

In this study, we used probabilistic ICA and ECM to investigate whether the core areas of the DMN (the temporally most coherent task-negative network) are also the most influential

Table 3

Pearson's correlations between average ECz of all RSNs

	1	2	3	4	5	6	7	8
DMN (1)								
Medial Visual (2)	-.466*							
Lateral Visual (3)	-.537**	.783***						
Auditory (4)	-.404*	-.226	-.065					
Frontoparietal left (5)	.373*	-.730***	-.638***	.178				
Frontoparietal right (6)	.438*	-.705*	-.592**	.148	.878***			
Sensory Motor (7)	-.437*	.414*	.501**	.252	-.530**	-.478*		
Occipital Pole (8)	-.072	.468*	.318	-.286	-.324	-.309	-.004	
Executive control (9)	.218	-.584**	-.575**	.266	.662***	.643***	-.294	-.310

*Pcorrected < 1.0E-2, **Pcorrected < 1.0E-5, ***Pcorrected < 1.0E-10

Note. P-values are Bonferroni corrected for multiple comparisons. DMN = default mode network.

brain areas during resting state. Our results show that the areas identified as most central do not coincide with the areas that constitute the DMN that is typically extracted by ICA. In fact, the medial and lateral occipital cortices, as well as the posterior dorsal precuneus, supramarginal gyrus (SMG), and postcentral gyrus were identified to have the highest EC during rest. Consistent with that, we showed that the medial and lateral visual network, rather than the DMN, were on average the most central RSNs and that their mean EC correlated negatively with the EC of the DMN.

Independent component analysis

The networks identified by group-ICA matched results of existing studies using either ICA or other methods to investigate connectivity patterns during rest. The DMN was composed of the PCC, MPFC, lateral temporal cortex, angular gyrus, ventral precuneus

(central precuneus in Margulies et al., 2009, or L/R5 and L/R6 as described in Luo et al., 2019), as well as the hippocampus and parts of the cerebellum, which is in concordance with our hypothesis and the

Figure 3

Scatterplots

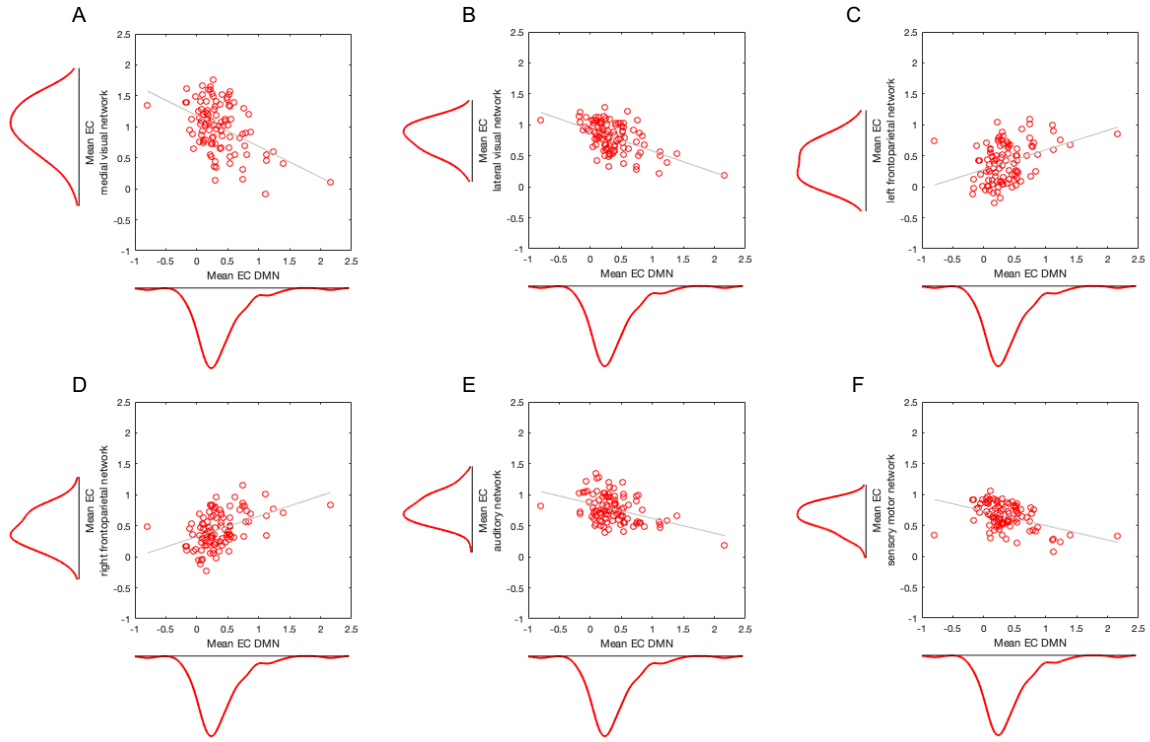

Note: Scatterplots and marginal densities of the weighted mean ECz (*N* = 100) of the DMN against (A) medial visual network, (B) lateral visual network, (C) left frontoparietal network, (D) right frontoparietal network, (E) auditory network, and (F) sensory motor network. DMN = default mode network, EC = eigenvector centrality.

typically reported DMN (Raichle et al., 2001; Buckner et al., 2008; Andrews-Hanna et al., 2014). Among the other 19 independent components, eight RSNs were identified (medial visual, lateral visual, auditory, left and right frontoparietal, sensory motor, occipital pole, executive control/salience network) that corresponded to networks described in other studies as well (e.g. Beckmann et al., 2005; Daimoiseaux et al., 2006; Smith et al., 2009; Laird et al.,

2011). The remaining components were classified to be either noise or components that spanned small subregions of sensory cortices and were not further analyzed.

While the DMN corresponded closely to earlier reports of existing RSNs, other components were less consistent with the literature. For example, in our results, the occipital pole is a separate RSN, which is not reported consistently (see e.g. Laird et al., 2011 and Smith et al., 2009 vs. Beckmann et al., 2005 and Yeo et al., 2011). Also, the current decomposition did not identify the cerebellum as one RSN, which is in line with a few (e.g. Beckmann et al., 2005; Yeo et al., 2011; Daimoiseaux et al., 2006), but not all studies (e.g. Laird et al., 2011; Smith et al., 2009). The absence of one coherent RSN in the cerebellum might be due to the distinct connectivity patterns of its subregions (Ren, Guo, & Guo, 2019), but this should be further investigated in future works. Finally, although the ninth RSN reported here, the executive control/salience network, spatially correlated significantly with the executive control network reported in Smith et al. (2009), its pattern corresponds less clearly to known RSNs than the other networks identified in the current study. Usually, the executive control network is composed of dorsolateral and -medial prefrontal areas, as well as the frontal eye field (Beckmann et al., 2005; Smith et al., 2009), while the salience network is described to comprise the insular cortex, dorsal anterior cingulate cortex, temporal pole, and amygdala (e.g. Seeley et al., 2007; Menon, 2011). The ninth RSN found here comprised areas of both, the salience and executive control network, which makes its interpretation somewhat ambiguous. Areas similar to the ones comprised in RSN 9 are sometimes referred to as one "task-positive network", associated with top-down attention modulation and working memory (e.g. Fox et al., 2005). However, the notion of only one task-positive network is debated (see e.g. Di & Biswal, 2014; Vincent et al., 2008; Smallwood, Brown, Baird, & Schooler, 2012) and RSN 9 does not entirely conform to that network. Thus, further investigation of the network would be needed to fully understand its interpretation and functional associations.

Eigenvector centrality mapping

The overall spatial layout of the ECM results differed considerably from the DMN identified by ICA. The highest EC was found in the precuneus, an area that is often referred to as centrality- and connectivity hub in the brain (e.g. van den Heuvel & Sporns, 2011; Hagmann et al., 2008; Tomasi & Volkow, 2011a; Bullmore & Sporns, 2009), and which is also frequently reported as part of the DMN, along with the neighboring PCC. However, it has been argued that the precuneus is in fact not part of the DMN (Buckner et al., 2008; Margulies et al., 2009) and recent studies exploring the functional parcellation of the area identified a more complex classification of the three (Margulies et al., 2009; Zhang & Li, 2012), or up to six (Luo et al., 2019) subparts of the precuneus. Specifically, only the ventral precuneus (Zhang & Li, 2012; or L/R5, L/R6 in Luo et al., 2019; central precuneus in Margulies et al., 2009) is functionally connected to areas of the DMN and other association areas, and corresponds to the division that is mostly reported, and here identified, as part of the DMN. In contrast, the division of the precuneus with the highest EC corresponds to the dorsal (posterior) precuneus (Zhang & Li, 2012; respectively L/R4 and L/R2 in Luo et al., 2019), which in turn shows functional connections to the adjacent visual network (Luo et al., 2019), negative connectivity to temporal gyri and parts of the cerebellum, and, when compared to the ventral precuneus, increased connections to occipital and parietal cortices (Zhang & Li, 2012). Thus, the most central part of the precuneus, as identified in our study, does not conform with the division of the precuneus associated with the DMN.

Another area that showed high EC during rest was the SMG of the inferior parietal lobe.

This area has been evidenced as centrality hub before (e.g. Liu et al., 2012; Tomasi & Volkow, 2011a; Tomasi & Volkow, 2011b) and generally appears to be involved in semantic processing (Chou et al., 2006), executive control of motor behavior (Kübler, Dixon, & Garavan, 2006), as well as somatosensory discrimination (Akatsuka et al., 2008). Beyond that, the SMG is sometimes referred to as part of the "temporo-parietal junction" (TPJ; a

converging point of the angular gyrus, SMG, and superior temporal gyrus), which in turn is related to bottom-up reorienting of attention, perception of the self, mind wandering, social cognition, and autobiographical memory retrieval (Igelström & Graziano, 2017). More specifically though, the SMG corresponds to the anterior subdivision of the TPJ (Igelström & Graziano, 2017) and is functionally connected to the anterior cingulate, anterior insular, inferior parietal lobe, and the thalamus (Zuo et al., 2012; Igelström & Graziano, 2017; Mars et al., 2011) – areas, which are referred to as attention control- (e.g. Zuo et al., 2012) or cingulo-opercular network (e.g. Sadaghiani & D'Esposito, 2014). In contrast, the angular gyrus or posterior subdivision of the TPJ (Igelström & Graziano, 2017) is functionally connected to areas of the DMN (Igelström & Graziano, 2017; Igelström, Webb, & Graziano, 2015; Mars et al., 2011; Zuo et al., 2012) and in turn did not appear as one of the most central areas in ECM.

The largest cluster with high EC was found in primary and secondary visual cortices (the cuneus, calcarine sulcus, and lateral occipital lobe), which was not expected based on the existing DMN literature. Still, high centrality in visual areas during rest has been reported before, albeit mostly incidentally and therefore not thoroughly discussed. For example, Tomasi and Volkow (2011a) identified the primary visual cortex along with the precuneus as global functional connectivity density hub, and the cuneus has been reported as cortical connectivity hub as well (Tomasi & Volkow, 2011b). A study comparing different centrality measures further showed that EC during rest was the highest in lateral and medial visual areas, the parieto-occipital sulcus, and around the TPJ (Zuo et al., 2012). Also, EC, when compared to degree centrality (DC), was higher in the medial visual cortex, while DC was higher in the PCC (Zuo et al., 2012). Finally, Cole and colleagues reported the visual regions among the globally most connected ones, and the cuneus and precuneus were mentioned as structural core regions in the brain (Cole, Pathak, & Schneider, 2010; Hagmann et al., 2008). Importantly, the aforementioned studies include both, "eyes open" and "eyes closed" rsfMRI acquisitions, which rules out the possibility that findings of high centrality in the visual cortex

are simply due to incoming visual information during "eyes open" data acquisition. Beyond research demonstrating high global centrality of occipital areas, studies have evidenced that the primary visual cortex shows significant fluctuations during rest, which were associated with activity in a network comprised of the middle occipital gyrus, cuneus, lingual gyrus, precuneus, pre- and postcentral gyrus (Wang et al., 2008; Nir et al., 2006), as well as parts of the temporal lobe (Wang et al., 2008). These task-free activation patterns, which widely overlap with the centrality hubs found in the current study, were associated with memory-related mental imagery and replaying information for visual memory consolidation (Wang et al., 2008). Lastly, a study showed that alcohol induction in healthy participants induced increases in functional connectivity and rsfMRI signal fluctuations in the visual network, and no other RSN (Esposito et al., 2010). This not only confirms the importance of the visual network during rest, but also suggests that it serves a more versatile and not strictly modular function.

Network centrality correlations

Reconfirming and broadening the aforementioned findings, we for the first time compared the EC of different RSNs and showed that the medial and lateral visual network were on average significantly more central than the DMN. More specifically, the weighted average of the EC in areas defined by every RSN's thresholded spatial ICA map indicated that the medial visual network was the most central network (and significantly more central than all other RSNs), while the DMN was significantly less central than all visual networks, the auditory network, and the sensory motor network. Furthermore, the average EC of the DMN was negatively correlated to the EC in the medial and lateral visual, sensory motor, and auditory network, while it correlated positively with the left and right frontoparietal network. At first glance, the positive correlation between the DMN and the frontoparietal networks might seem counterintuitive, as correlations between task-positive networks and the DMN are usually reported to be negative (e.g. Fox et al., 2005; see Anticevic et al., 2012 for a review).

However, the relation between the DMN and the frontoparietal network (FPN) in particular has been demonstrated to be more complex, by studies showing their positive functional coupling (Spreng et al., 2010) and their cooperation to manage external and internal trains of thoughts (Smallwood et al., 2012). Importantly, functional coupling, i.e. the temporal internetwork correlation, is not equivalent to the correlation between centralities of different networks shown here. While the former directly reflects joint fluctuations of BOLD activity at a particular point in time, the latter indicates how the average centralities *across time* relate to each other. Thus, although our results might support the assumption of cooperation between DMN and FPN during rest by showing that high centrality of the former is generally accompanied by high centrality of the latter, future work is needed to confirm this. Specifically, dynamic EC correlations between the different RSNs should be investigated to understand how their importance behaves and relates to each other at specific points in time.

The negative correlation between the DMN and medial and lateral visual network (VN) shows that their centrality during rest was reversed – overall low centrality in the DMN was accompanied by high centrality in the VNs, and vice versa. Negative correlations between the primary visual cortex and the DMN during rest have been shown before (Scheeringa et al., 2012) and there is more evidence for functional coupling of primary visual areas and the DMN in association to visual mental imagery (Zhang et al., 2018). Also, both the DMN and VNs have been shown to be at the highest level of the hierarchical modular organization of the brain during rest (Meunier et al., 2009). Together with our finding that the medial VN is the most central, this evidence might suggest that the negative centrality correlation points to an interplay between the DMN and VN, in which the latter plays a dominant role. We further propose a functional interpretation of the appearing predominance of the VNs, in which the VNs are involved in the monitoring of incoming stimuli and internal processing during rest. Relevant evidence for this interpretation comes from (i) research showing VN aberrancies in clinical conditions associated with increased levels of trait

impulsivity ("the tendency to act quickly without considering the broader […] consequences of one's actions", Davis et al., 2012), (ii) research suggesting that trait impulsivity is related to anomalies in VN activity and connectivity, and (iii) the existing notion that neural alpha oscillations (8-12 Hz) in the occipital cortex facilitate internal processing by gating incoming stimuli during rest. The three aspects are elaborated in the following.

Firstly, AD, ASD, bipolar disorder, schizophrenia, and ADHD have been associated with deviant connectivity of the VNs during rest. For example, decreased functional connectivity (Lehmann et al., 2015; Binnewijzend et al., 2012; Sanz-Arigita et al., 2010), regional homogeneity (ReHo) (Cui et al., 2016), and EC (Binnewijzend et al., 2014; Adriaanse et al., 2016) of the lateral and medial VN have been found in AD and bipolar disorder. Reduced nodal efficiency and increased ReHo in the medial occipital cortex during rest have been associated to ADHD (Wang et al., 2009; Cao et al., 2006) and medial VN connectivity, as well as connections of the VN to the DMN were found to be essential for the diagnostic classification and symptom severity of ASD (Chen et al., 2015; Keown et al., 2013). The connectivity between VN and DMN has also been associated to positive symptoms in schizophrenia (disorganized thought and behavior; Meda et al., 2012). Importantly, all aforementioned conditions are also commonly associated with increased trait impulsivity (Najt et al., 2007; Rochat et al., 2008; Mayes, Calhoun, Mayes, & Molitoris, 2012; Wistanley, Eagle, & Robbins, 2006; Ouzir, 2013), which ties in with the second line of evidence: Research suggests that impulsivity is associated with anomalies of VN connectivity. High trait impulsivity has been related to changes in resting state connectivity of the medial and lateral VN in healthy participants (Davis et al., 2012) and to connectivity of lateral visual areas to the amygdala in abstinent heroin dependent subjects (Xie et al., 2011). Better inhibitory control was further related to increased ReHo in the medial VN (Tian, Ren, & Zang, 2012) and reduced gray matter volume in the parieto-occipital sulcus was shown in subjects with high trait impulsivity (Ide et al., 2017). Also, inhibitory control in children with

ADHD has been related to connections of the VN to the cingulo-opercular network and connectivity between the DMN and cuneal cortex was related to impulsivity in typical developing children (Mennes et al., 2011; Inuggi et al., 2014). Lastly, a review of the phenotypic associations of different RSNs has emphasized the relation of the VN to affective states and emotional functioning, specifically to impulsive behavior and inhibitory control (Vaidya & Gordon, 2013).

At last, all abovementioned conditions associated with VN anomalies (ADHD, AD, ASD, schizophrenia, and bipolar disorder) also show decreased occipital alpha activity during rest (Woltering, Jung, Liu, & Tannock, 2012; Başar et al., 2012; Osipova et al., 2005; Wang et al., 2013; Goldstein et al., 2015). Power in the occipital alpha frequency band is suggested to facilitate internal processing by gating incoming stimuli (e.g. Mo, Liu, Huang, & Ding, 2013; Klimesch, Sauseng, & Hanslmayr, 2007), which is based on the link between alpha oscillations and decreased cortical excitability, inhibition of task irrelevant cortical regions, and attention modulation (Mayhew, Ostwald, Porcaro, & Bagshaw, 2013; Capotosto, Babiloni, Romani, & Corbetta, 2009; Klimesch et al., 2007; Palva & Palva, 2007). Evidence for positive correlations between occipital alpha oscillations and DMN BOLD activity further corroborates the notion that they facilitate internal processing during rest (Jann et al., 2010; Knyazev, Slobodskoj-Plusnin, Bocharov, & Pylkova, 2011; Mo et al., 2013). Importantly, alpha oscillations have been shown to mainly source in the occipital cortex (e.g. Hari et al., 1997; Moosman et al., 2003).

All in all, given that evidence strongly suggests the relation between connectivity of the VNs and trait impulsivity, their predominance shown in the current study might point to a role of the VNs in regulating impulsivity and premeditation during rest, i.e. balancing incoming stimuli and internal processing. In other words, our findings might be another manifestation of the mechanism proposed for occipital alpha oscillations, where high EC of the VNs would indicate enhanced occipital alpha power, i.e. efficient dampening of external

stimuli, decreased impulsivity, and accompanied BOLD activity in the DMN (note here that *activity* is not equal to *centrality*). In contrast, low EC of the VNs would indicate lower alpha power, i.e. increased cortical excitability and decreased DMN activity. The negative correlation between the EC of VN and DMN might thus point to a cooperation, in which global connectivity of the VNs (rather than the DMN) is maintained to facilitate appropriate regulation of higher order network activity via global connections.

Other research is in line with this interpretation. For example, evidence suggests that during rest, the occipital gyrus modulates interactions between DMN and dorsal attention network, as well as interactions between anterior and posterior DMN (Di & Biswal, 2014). Also, there is evidence for the link between occipital alpha power and resting state connectivity in general, within the visual system, and between visual and ventral medial prefrontal areas (Tagliazucchi et al., 2012; Scheeringa et al., 2012). However, the current results are not sufficient to develop a thorough model and it should be noted that the aforementioned studies show decreased rather than increased connectivity of occipital regions in response to high alpha-power. Also, whether there is an association between alpha power and EC (of the VN) in particular is unanswered. Generally, future work should further investigate the role of the medial and lateral VN during rest. Considering that typically, the FPN is reported with regard to attention modulation and inhibitory control (e.g. Marek & Dosenbach, 2018; Chadick & Gazzaley, 2011), and the salience network (specifically the insula) with regard to network switching (e.g. Sridharan, Levitin, & Menon, 2008), their relation to the VN should be researched as well. Finally, dynamic EC and the according changes in (effective) connectivity of the two visual RSNs should be explored to identify their separate roles, and the relation between EC, metabolic activity, and local connectivity should be analyzed to further incorporate the current results into the existing literature.

Functional connectivity in ECM and ICA

Our study demonstrates that ECM and ICA extract different aspects of intrinsic functional connectivity in the brain and that the two methods can be meaningfully combined with the here explored analyses. We showed that ECM derives a different resting state connectivity pattern than the DMN extracted by ICA and we thereby highlighted the aspects of resting state connectivity that these methods distinguish: ICA enables to understand the entire data at once and extracts multiple independent, temporally coherent networks from the brain, among which the DMN. In contrast, ECM considers the whole brain as a network, and derives *one global* description of its intra-connectivity. Therefore, the most central regions extracted by ECM can be less understood as one coherent neurobiological entity, like the RSNs extracted by ICA, but rather as an independent description of the most influential areas across space and time, i.e. across networks (see similarly also McKeown et al. (1998) and Cole et al. (2010) for a discussion and comparison of PCA as opposed to ICA for fMRI analyses). All in all, ECM is an analysis technique which provides a global perspective and straightforward interpretation of the brain's connectivity organization during any cognitive state. By comparing the average centrality of RSNs identified by ICA, ECM can be combined with ICA and the two methods can be interpreted cohesively.

Limitations

The spatial smoothing applied to the rsfMRI data, as well as the interpolation during resampling could have led to artificially increased temporal correlations between neighboring voxels. However, the same resampling and smoothing has been applied to the data used in both analysis methods, which rules out that it had an impact on the difference between the results of the two. Secondly, the inherent preprocessing of ICA included temporal demeaning and variance normalization. These steps are not required for ECM, but the lack of application to the data used for ECM could have potentially led to differences between the respective results, although unlikely. Thirdly, we only included a limited amount of the components extracted by ICA in our analyses. In the future, a more extensive comparison of EC in various

networks could be addressed to enable a more overarching understanding of their interactions. Fourthly, the current ECM results exceeded conventional significance levels, which available tools were unable to capture. Although a higher than traditionally used number of permutations (1,000,000) in a nonparametric t-test was applied, the range of significance was restricted, as an overall ceiling p-value was reached in most voxels. Future studies should consider increasing computational power to enable a higher number of permutations and hence a more precise estimate of significance. Lastly, we did not further explore the functional connectivity of the most central areas during rest, which should be done in future works to better understand the connectivity organization of those regions.

Conclusion

To conclude, this study shows that ICA and ECM, when applied to the same rsfMRI data with the same pre-processing, reveal different spatial maps of the most prominent areas during resting state. The DMN does not conform with the most central areas during rest, which demonstrates that ECM and ICA reveal distinct aspects of resting state connectivity. We show that the medial and lateral VN are the most central RSNs during rest and propose a mechanistic explanation, in which the VNs are involved in monitoring incoming stimuli and internal processing. Altogether, our results suggest that the investigation of individual variation in VNs is more important than previously believed and they further motivate future work exploring the relative EC of different RSNs as a potential neuromarker for diagnostic applications. The exceedingly high significance and large effect sizes of the current findings are particularly promising for personalized applications.

Acknowledgments

Data were provided by the Human Connectome Project, WU-Minn Consortium (Principal Investigators: David Van Essen and Kamil Ugurbil; 1U54MH091657) funded by the 16 NIH Institutes and Centers that support the NIH Blueprint for Neuroscience Research; and by the McDonnell Center for Systems Neuroscience at Washington University. Brain

surfaces were visualized with the BrainNet Viewer (Xia, Wang, & He, 2013, http://www.nitrc.org/projects/bnv/).

Appendix

Figure A1

Nine ICA components

DMN

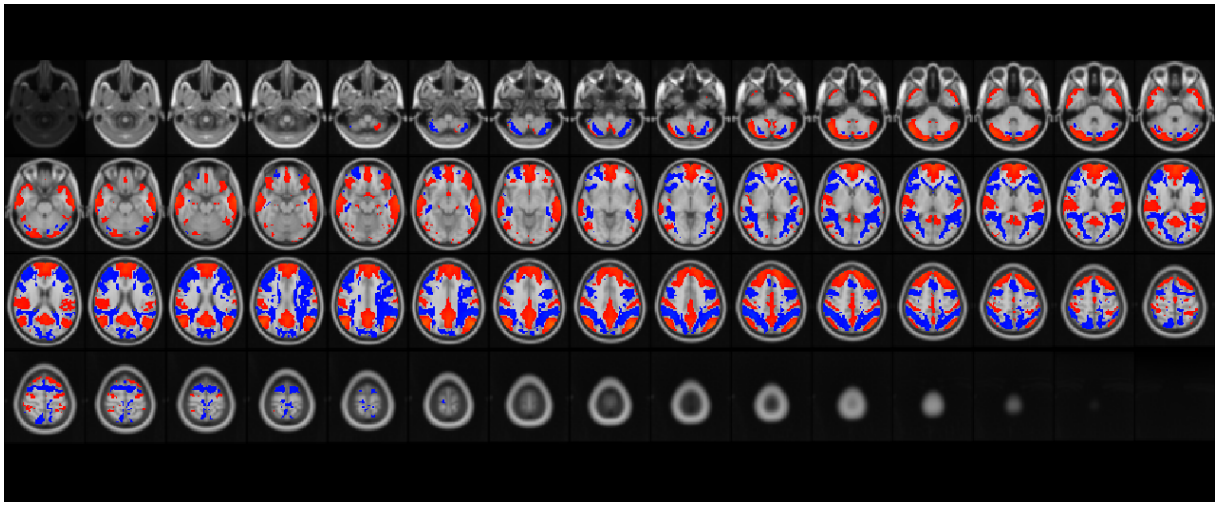

Medial visual network

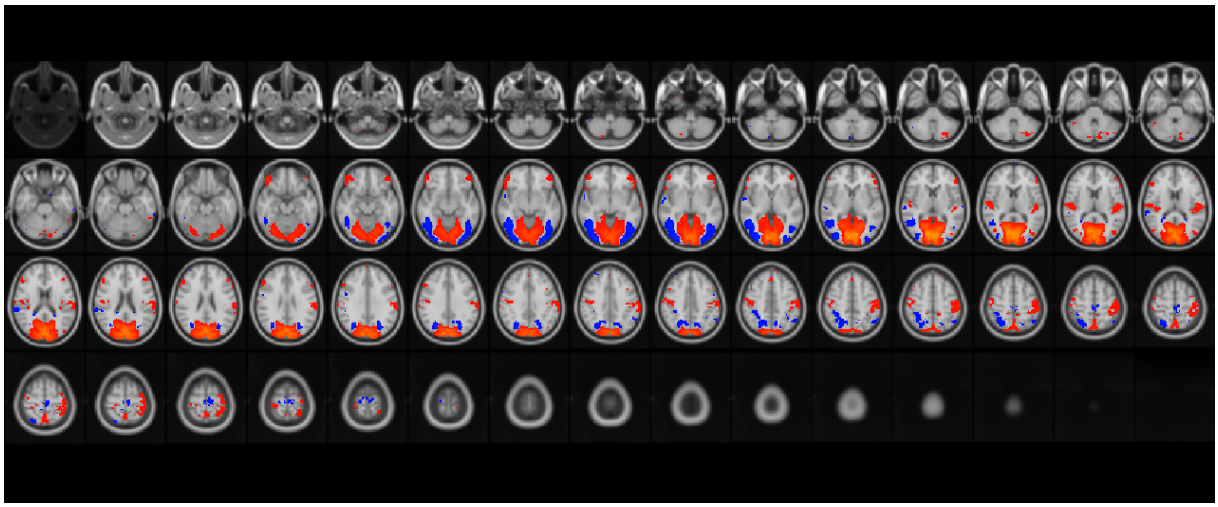

Lateral visual network

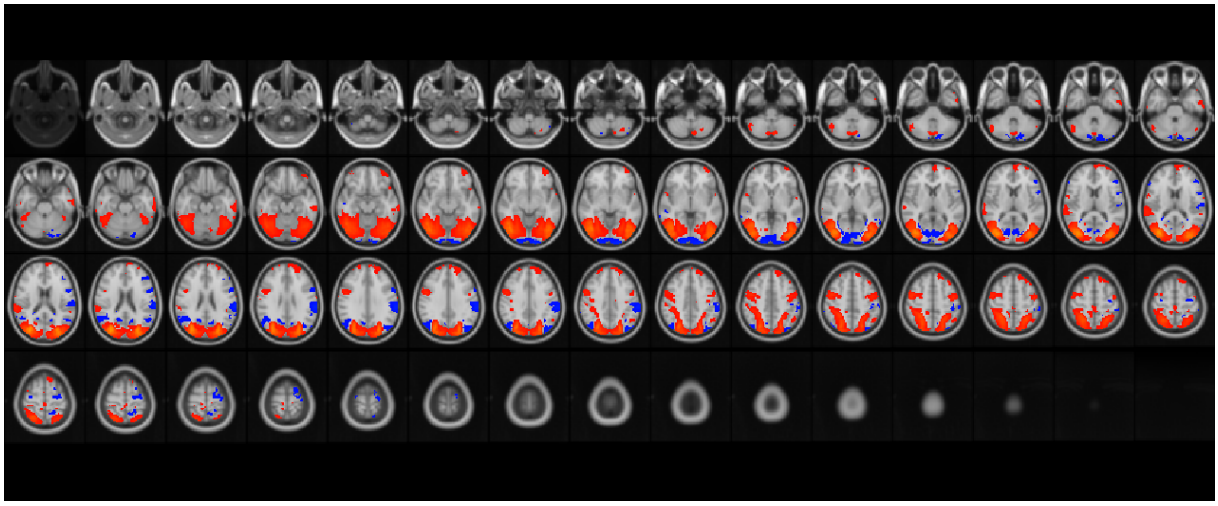

Auditory network

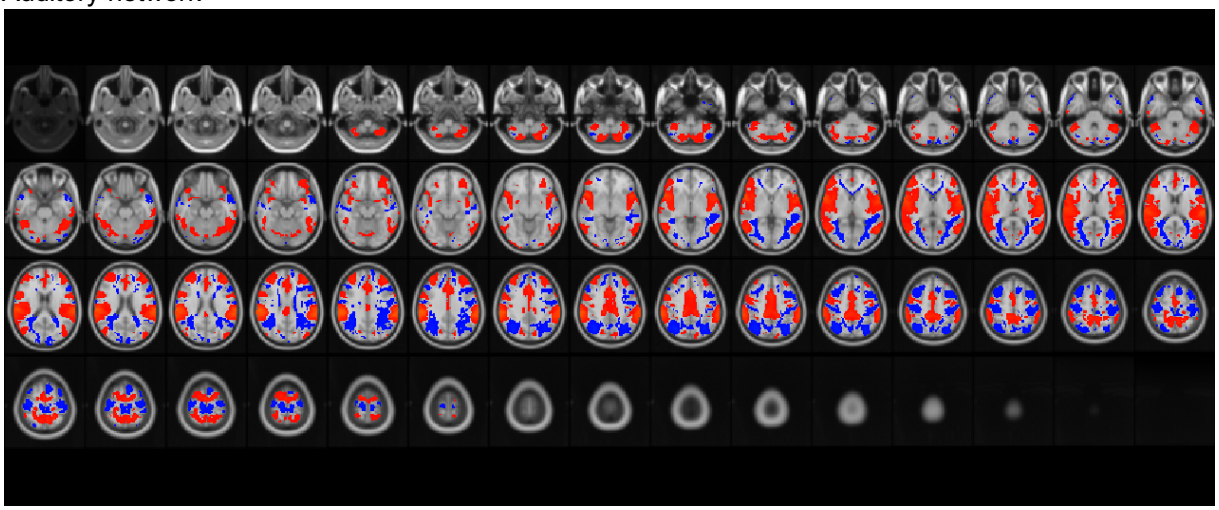

Right frontoparietal network

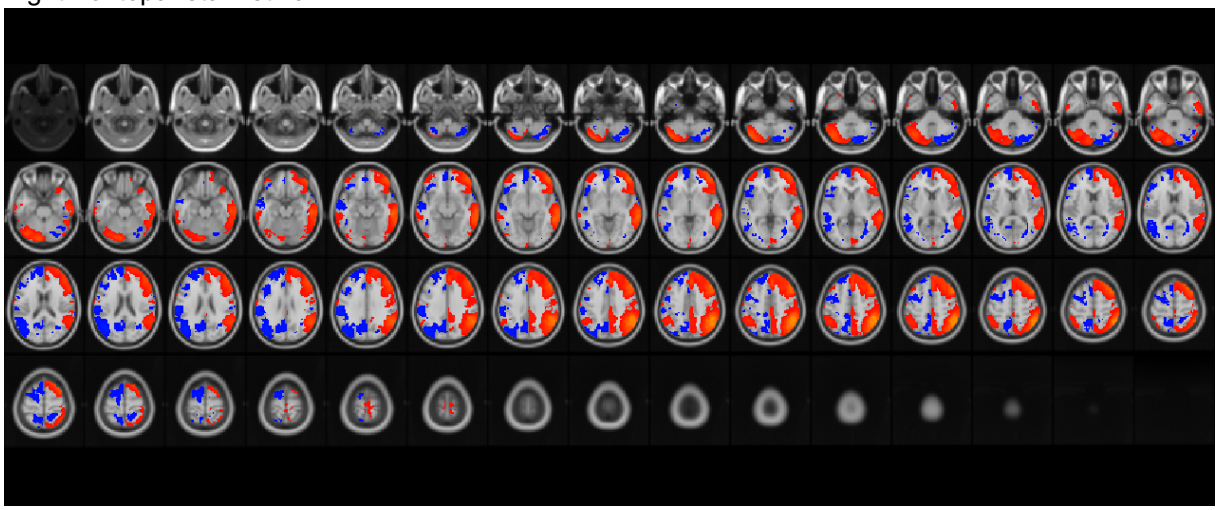

Left frontoparietal network

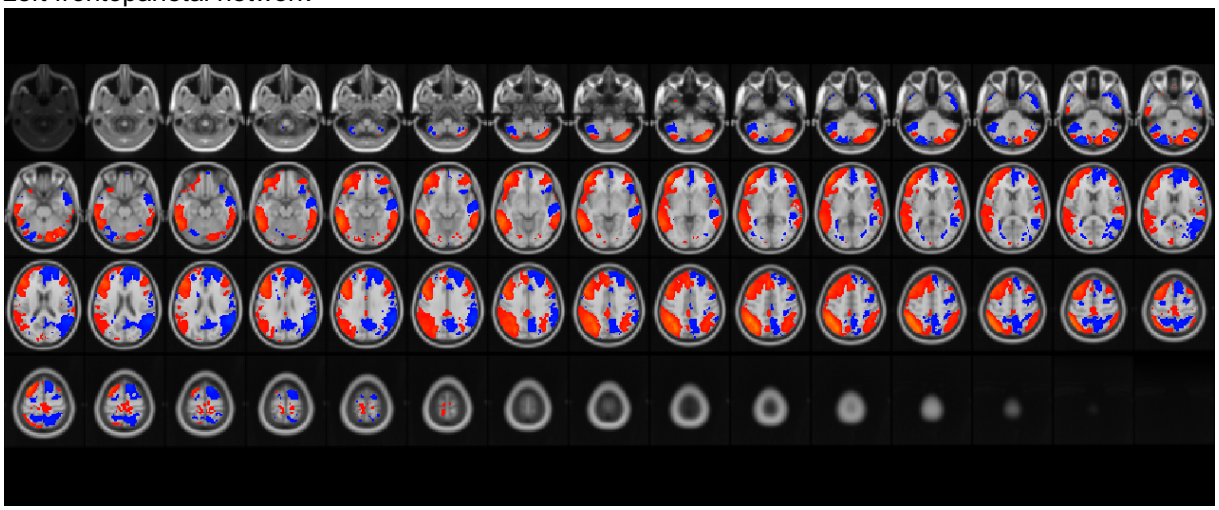

Sensory motor network

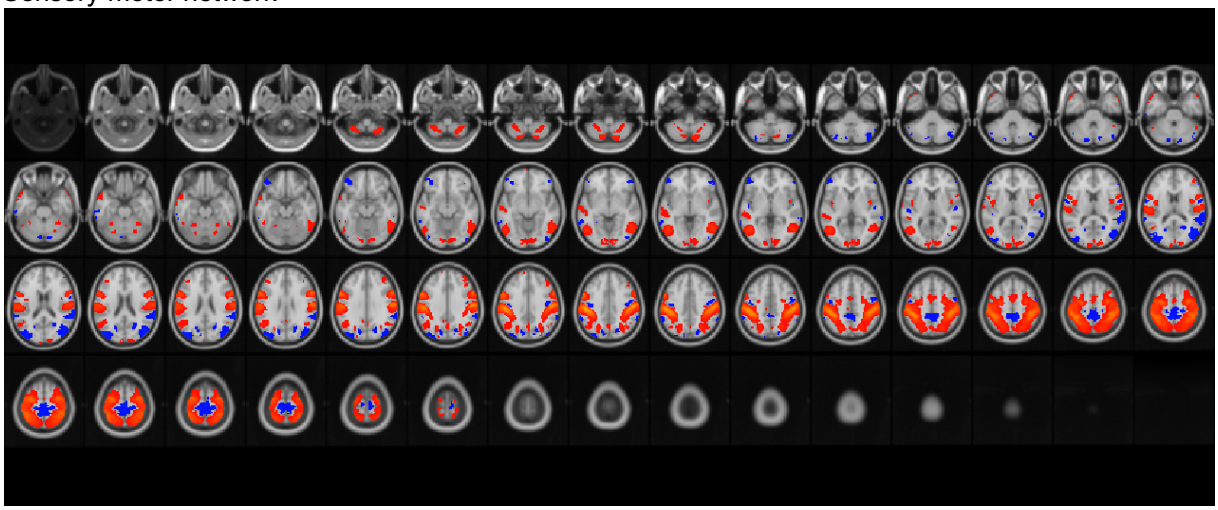

Occipital pole network

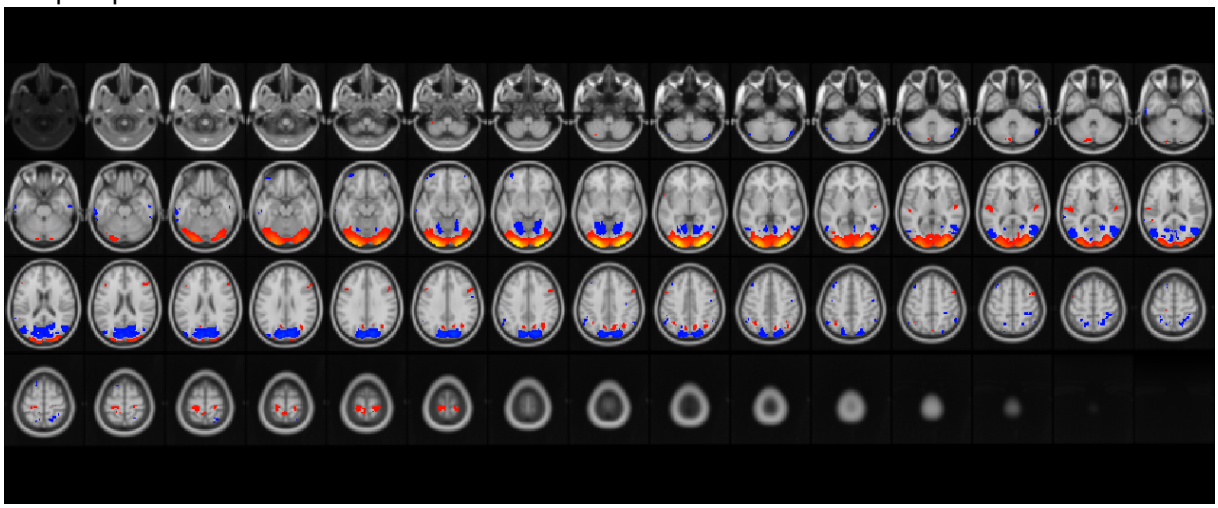

Executive control/salience network

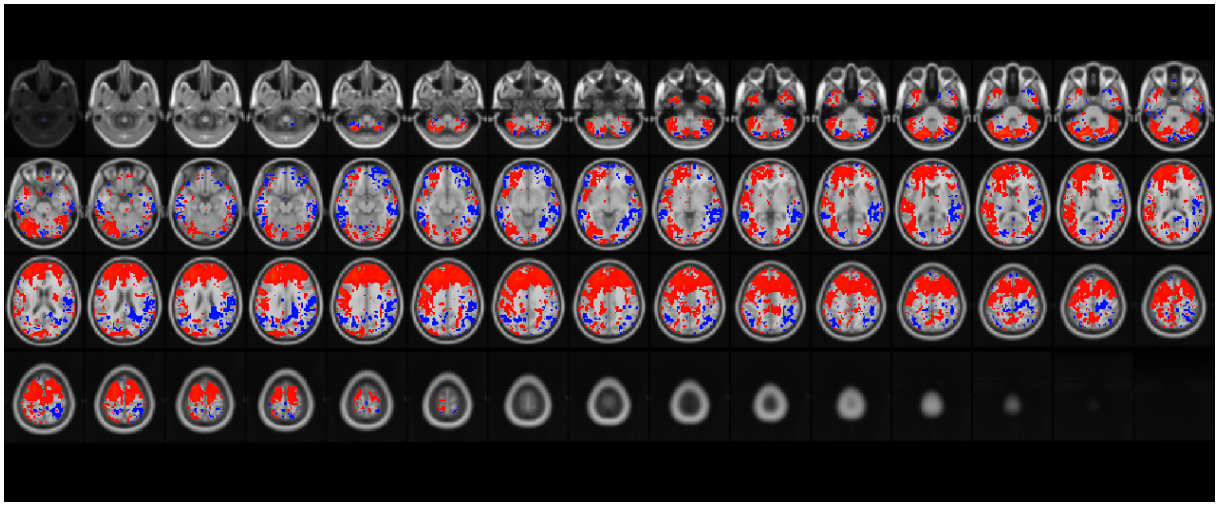

Note. Thresholded Z-maps of nine independent components estimated by probabilistic group ICA (*d* = 20) of 100 healthy subjects. Positive (red) and negative (blue) Z-values are displayed on slices of a MNI152 T1 structural. Thresholding was done by fitting a Gaussian/gamma mixture model to the data, with P > 0.5.

Table A1

Pairwise comparisons

RSN	*T* (df = 99) against medial visual	*P* against medial visual (Bonferroni corrected)	*T* (df = 99) against lateral visual	*P* against lateral visual (Bonferroni corrected)
DMN	9.680	1.963E-14	8.126	4.634E-11
Medial Visual	-	-	7.749	2.967E-10
Lateral Visual	7.749	2.967E-10	-	-
Auditory	4.508	0.001	0.726	ns
Frontoparietal left	9.080	3.993E-13	8.017	7.948E-11
Frontoparietal right	8.809	1.553E-12	7.618	5.643E-10
Sensory Motor	9.598	2.966E-14	6.739	3.838E-8
Occipital Pole	10.676	1.327E-16	6.027	1.000E-5
Salience	12.958	8.954E-33	12.952	2.441E-37

Note. The mean ECz of the medial and lateral visual network was compared to the mean EC of every other RSN. ns = non-significant, DMN = default mode network.

References

Adriaanse, S. M., Wink, A. M., Tijms, B. M., Ossenkoppele, R., Verfaillie, S. C., Lammertsma, A. A., . . . Barkhof, F. (2016). The Association of Glucose Metabolism and Eigenvector Centrality in Alzheimer's Disease. *Brain Connectivity, 6*(1), 1-8. doi:10.1089/brain.2014.0320

Akatsuka, K., Noguchi, Y., Harada, T., Sadato, N., & Kakigi, R. (2008). Neural codes for somatosensory two-point discrimination in inferior parietal lobule: An fMRI study. *NeuroImage, 40*(2), 852-858. doi:10.1016/j.neuroimage.2007.12.013

Algina, J. & Keselman, H.J. (1997). Detecting repeated measures effects with univariate and multivariate statistics. *Psychological methods, 2*, 208-218.

Alnæs, D., Sneve, M.H., Richard, G., Skåtun, K.C., Kaufmann, T., Nordvik, J.E., Kaufmann, T., …, Westlye, L.T. (2015). Functional connectivity indicates differential roles for the intraparietal sulcus and the superior parietal lobule in multiple object tracking. *Neuroimage, 123*, 129–37.

Andrews-Hanna, J. R., Reidler, J.S., Sepulcre, J., Poulin, R., & Buckner, R.L. (2010). Functional-anatomic fractionation of the brain's default network. *Neuron, 65*, 550–62.

Andrews-Hanna, J. R., Smallwood, J., & Spreng, R. N. (2014). The default network and self-generated thought: Component processes, dynamic control, and clinical relevance. *Annals of the New York Academy of Sciences,1316*(1), 29-52. doi:10.1111/nyas.12360

Anticevic, A., Cole, M. W., Murray, J. D., Corlett, P. R., Wang, X., & Krystal, J. H. (2012). The role of default network deactivation in cognition and disease. *Trends in Cognitive Sciences, 16*(12), 584-592. doi:10.1016/j.tics.2012.10.008

Başar, E., Güntekin, B., Atagün, I., Gölbaşı, B. T., Tülay, E., & Özerdem, A. (2012). Brain's alpha activity is highly reduced in euthymic bipolar disorder patients. *Cognitive Neurodynamics, 6*(1), 11-20. doi:10.1007/s11571-011-9172-y

Beckmann, C. F. (2012). Modelling with independent components. *NeuroImage*, *62*(2), 891–901. doi: 10.1016/j.neuroimage.2012.02.020

Beckmann, C. F., DeLuca, M., Devlin, J. T., & Smith, S. M. (2005). Investigations into resting-

state connectivity using independent component analysis. *Philos. Trans. R. Soc. Lond. B Biol. Sci., 360,* 1001–1013.

Beckmann, C. F. & Smith, S. M. (2004). Probabilistic independent component analysis for functional magnetic resonance imaging. *IEEE Trans. Med. Imaging 23,* 137–152.

Binnewijzend, M.A.A, Schoonheim, M.M., Sanz-Arigita, E., Wink, A.M., van der Flier, W.M., Tolboom, N., Adriaanse, S.M., … Barkhof, F. (2012). Resting-state fMRI changes in Alzheimer's disease and mild cognitive impairment. *Neurobiology of Aging, 33*, 2018-2028. doi: 10.1016/j.neurobiolaging.2011.07.003

Binnewijzend, M. A., Adriaanse, S. M., Flier, W. M., Teunissen, C. E., Munck, J. C., Stam, C. J., . . . Wink, A. M. (2014). Brain network alterations in Alzheimer's disease measured by Eigenvector centrality in fMRI are related to cognition and CSF biomarkers. *Human Brain Mapping, 35*(5), 2383-2393. doi:10.1002/hbm.22335

Biswal, B., Yetkin, F.Z., Haughton, V.M., & Hyde, J.S. (1995). Functional connectivity in the motor cortex of resting human brain using echo-planar MRI. *Magn. Res. Med, 34*, 537–541.

Bluhm, R. L., Osuch, E. A., Lanius, R. A., Boksman, K., Neufeld, R. W., Théberge, J., & Williamson, P. (2008). Default mode network connectivity: effects of age, sex, and analytic approach. *NeuroReport*, *19*(8), 887–891. doi: 10.1097/wnr.0b013e328300ebbf

Bonacich, P. (1972). Factoring and weighting approaches to clique identification. *Journal of Mathematical Sociology, 2*, 113–120.

Broyd, S. J., Demanuele, C., Debener, S., Helps, S. K., James, C. J., & Sonuga-Barke, E. J.

(2009). Default-mode brain dysfunction in mental disorders: A systematic review. *Neuroscience & Biobehavioral Reviews, 33*(3), 279-296. doi:10.1016/j.neubiorev.2008.09.002

Buckner, R. L., Andrews-Hanna, J. R., & Schacter, D. L. (2008). The Brain's Default Network. *Annals of the New York Academy of Sciences, 1124*(1), 1-38. doi:10.1196/annals.1440.011

Buckner, R. L., Sepulcre, J., Talukdar, T., Krienen, F. M., Liu, H., Hedden, T., . . . Johnson, K. A. (2009). Cortical Hubs Revealed by Intrinsic Functional Connectivity: Mapping, Assessment of Stability, and Relation to Alzheimer's Disease. *Journal of Neuroscience, 29*(6), 1860-1873. doi:10.1523/jneurosci.5062-08.2009

Bullmore, E., & Sporns, O. (2009). Erratum: Complex brain networks: Graph theoretical analysis of structural and functional systems. *Nature Reviews Neuroscience, 10*(4), 312-312. doi:10.1038/nrn2618

Cao, Q., Zang, Y., Sun, L., Sui, M., Long, X., Zou, Q., & Wang, Y. (2006). Abnormal neural activity in children with attention deficit hyperactivity disorder: A resting-state functional magnetic resonance imaging study. *NeuroReport,17*(10), 1033-1036. doi:10.1097/01.wnr.0000224769.92454.5d

Capotosto, P., Babiloni, C., Romani, G. L., & Corbetta, M. (2009). Frontoparietal Cortex Controls Spatial Attention through Modulation of Anticipatory Alpha Rhythms. *Journal of Neuroscience, 29*(18), 5863-5872. doi:10.1523/jneurosci.0539-09.2009

Chadick, J. Z., & Gazzaley, A. (2011). Differential coupling of visual cortex with default or frontal-parietal network based on goals. *Nature Neuroscience, 14*(7), 830-832. doi:10.1038/nn.2823

Chen, C. P., Keown, C. L., Jahedi, A., Nair, A., Pflieger, M. E., Bailey, B. A., & Müller, R.

(2015). Diagnostic classification of intrinsic functional connectivity highlights somatosensory, default mode, and visual regions in autism. *NeuroImage: Clinical, 8*, 238-245. doi:10.1016/j.nicl.2015.04.002

Chou, T., Booth, J. R., Bitan, T., Burman, D. D., Bigio, J. D., Cone, N. E., . . . Cao, F. (2006). Developmental and skill effects on the neural correlates of semantic processing to visually presented words. *Human Brain Mapping, 27*(11), 915-924. doi:10.1002/hbm.20231

Cole, D.M., Smith, S.M., & Beckmann, C.F., (2010). Advances and pitfalls in the analysis and interpretation of resting-state fmri data. *Front. Syst. Neurosci. 4*, 8.

Cole, M. W., Pathak, S., & Schneider, W. (2010). Identifying the brain's most globally connected regions. *NeuroImage,49*(4), 3132-3148. doi:10.1016/j.neuroimage.2009.11.001

Comon, P. (1994). Independent component analysis — a new concept? *Signal Process., 36*, 287–314.

Cui, D., Gao, W., Jiao, Q., Cao, W., Qi, R., Guo, Y., … Lu, G. (2016). Abnormal Resting-State Regional Homogeneity Relates to Cognitive Dysfunction in Manic Bipolar Disorder Adolescents: An fMRI Study. *Journal of Medical Imaging and Health Informatics*, *6*(7), 1673–1678. doi: 10.1166/jmihi.2016.1870

Damoiseaux, J.S., Rombouts, S.A.R.B., Barkhof, F., Scheltens, P., Stam, C.J., Smith, S.M., & Beckmann, C.F. (2006). Consistent resting-state networks across healthy subjects. *Proc. Natl. Acad. Sci. U.S.A., 103*, 13848–13853.

Davis, F. C., Knodt, A. R., Sporns, O., Lahey, B. B., Zald, D. H., Brigidi, B. D., & Hariri, A. R. (2012). Impulsivity and the Modular Organization of Resting-State Neural Networks. *Cerebral Cortex, 23*(6), 1444-1452. doi:10.1093/cercor/bhs126

Di, X., & Biswal, B. B. (2014). Modulatory interactions between the default mode network and task positive networks in resting-state. doi:10.7287/peerj.preprints.124

Esposito, F., Pignataro, G., Renzo, G. D., Spinali, A., Paccone, A., Tedeschi, G., & Annunziato, L. (2010). Alcohol increases spontaneous BOLD signal fluctuations in the visual network. *NeuroImage, 53*(2), 534-543. doi:10.1016/j.neuroimage.2010.06.061

Filippini, N., Macintosh, B., Hough, M., Goodwin, G., Frisoni, G., Ebmeier, K., . . . Mackay, C. (2009). Distinct patterns of brain activity in young carriers of the APOE e4 allele. *NeuroImage, 47*. doi:10.1016/s1053-8119(09)71381-3

Fischl, B. (2012). FreeSurfer. *NeuroImage, 62*, 774-781.

Fox, M. D., Snyder, A. Z., Vincent, J. L., Corbetta, M., Van Essen, D. C., & Raichle, M. E. (2005). The human brain is intrinsically organized into dynamic, anticorrelated functional networks. *Proc. Natl. Acad. Sci. U.S.A.*, *102*, 9673–8.

Glasser, M.F. Stamatios, N., Sotiropoulos, J., Wilson, A., Coalson, T. S., Fischl, B., … Jenkinson, M. (2013). The minimal preprocessing pipelines for the Human Connectome Project. *NeuroImage, 80*, 105-124.

Goldstein, M. R., Peterson, M. J., Sanguinetti, J. L., Tononi, G., & Ferrarelli, F. (2015). Topographic deficits in alpha-range resting EEG activity and steady state visual evoked responses in schizophrenia. *Schizophrenia Research,168*(1-2), 145-152. doi:10.1016/j.schres.2015.06.012

Golub, G. & van Loan, C. (1996). *Matrix computations*. Baltimore, MD: Johns Hopkins University Press, 3rd edition.

Greicius, M. D., Flores, B. H., Menon, V., Glover, G. H., Solvason, H. B., Kenna, H., . . . Schatzberg, A. F. (2007). Resting-State Functional Connectivity in Major Depression: Abnormally Increased Contributions from Subgenual Cingulate Cortex and Thalamus. *Biological Psychiatry, 62*(5), 429-437. doi:10.1016/j.biopsych.2006.09.020

Hadriche, A., Jmail, N., Blanc, J., & Pezard, L. (2019). Using centrality measures to extract

core pattern of brain dynamics during the resting state. *Computer Methods and Programs in Biomedicine, 179*, 104985. doi:10.1016/j.cmpb.2019.104985

Hafkemeijer, A., Grond, J. V., & Rombouts, S. A. (2012). Imaging the default mode network in aging and dementia. *Biochimica Et Biophysica Acta (BBA) - Molecular Basis of Disease, 1822*(3), 431-441. doi:10.1016/j.bbadis.2011.07.008

Hagmann, P., Cammoun, L., Gigandet, X., Meuli, R., Honey, C. J., Wedeen, V. J., & Sporns, O. (2008). Mapping the Structural Core of Human Cerebral Cortex. *PLoS Biology, 6*(7). doi:10.1371/journal.pbio.0060159

Hari, R., Salmelin, R., Mäkelä, J., Salenius, S., & Helle, M. (1997). Magnetoencephalographic cortical rhythms. *International Journal of Psychophysiology, 26*(1-3), 51-62. doi:10.1016/s0167-8760(97)00755-1

Hartvig, N. & Jensen, J. (2000). Spatial mixture modelling of fMRI data. *Human Brain Mapping, 11*, 233–248.

Hove, M. J., Stelzer, J., Nierhaus, T., Thiel, S. D., Gundlach, C., Margulies, D. S., … Merker, B. (2015). Brain Network Reconfiguration and Perceptual Decoupling During an Absorptive State of Consciousness. *Cerebral Cortex*, *26*, 3116–3124. doi: 10.1093/cercor/bhv137

Hyvärinen, A. & Oja, E. (1997). A fast fixed-point algorithm for independent component analysis. *Neural Comput. 9*, 1483–1492.

Igelström, K. M., & Graziano, M. S. (2017). The inferior parietal lobule and temporoparietal junction: A network perspective. *Neuropsychologia, 105*, 70-83. doi:10.1016/j.neuropsychologia.2017.01.001

Igelström, K. M., Webb, T. W., & Graziano, M. S. (2015). Neural Processes in the Human Temporoparietal Cortex Separated by Localized Independent Component Analysis. *Journal of Neuroscience, 35*(25), 9432-9445. doi:10.1523/jneurosci.0551-15.2015

Inuggi, A., Sanz-Arigita, E., Gonzã¡lez-Salinas, C., Valero-Garcãa, A. V., Garcãa-Santos, J.

M., & Fuentes, L. J. (2014). Brain functional connectivity changes in children that differ in impulsivity temperamental trait. *Frontiers in Behavioral Neuroscience, 8*. doi:10.3389/fnbeh.2014.00156

Jann, K., Kottlow, M., Dierks, T., Boesch, C., & Koenig, T. (2010). Topographic Electrophysiological Signatures of fMRI Resting State Networks. *PLoS ONE, 5*(9). doi:10.1371/journal.pone.0012945

Jenkinson, M., Beckmann, C.F., Behrens, T.E., Woolrich, M.W., & Smith, S.M. (2012). FSL. *NeuroImage, 62*, 782-790.

Joyce, K. E., Laurienti, P. J., Burdette, J. H., & Hayasaka, S. (2010). A New Measure of Centrality for Brain Networks. *PLoS ONE, 5*(8). doi:10.1371/journal.pone.0012200

Kennedy, D. P., Redcay, E., & Courchesne, E. (2006). Failing to deactivate: Resting functional abnormalities in autism. *Proceedings of the National Academy of Sciences, 103*(21), 8275-8280. doi:10.1073/pnas.0600674103

Keown, C., Shih, P., Nair, A., Peterson, N., Mulvey, M., & Müller, R. (2013). Local Functional Overconnectivity in Posterior Brain Regions Is Associated with Symptom Severity in Autism Spectrum Disorders. *Cell Reports, 5*(3), 567-572. doi:10.1016/j.celrep.2013.10.003

Kernbach, J. M., Yeo, B. T., Smallwood, J., Margulies, D. S., Schotten, M. T., Walter, H., . . . Bzdok, D. (2018). Subspecialization within default mode nodes characterized in 10,000 UK Biobank participants. *Proceedings of the National Academy of Sciences, 115*(48), 12295-12300. doi:10.1073/pnas.1804876115

Klimesch, W., Sauseng, P., & Hanslmayr, S. (2007). EEG alpha oscillations: The inhibition–timing hypothesis. *Brain Research Reviews, 53*(1), 63-88. doi:10.1016/j.brainresrev.2006.06.003

Knyazev, G. G., Slobodskoj-Plusnin, J. Y., Bocharov, A. V., & Pylkova, L. V. (2011). The

default mode network and EEG alpha oscillations: An independent component analysis. *Brain Research, 1402*, 67-79. doi:10.1016/j.brainres.2011.05.052

Koch, W., Teipel, S., Mueller, S., Buerger, K., Bokde, A.L., Hampel, H., Coates, U., Reiser, M., & Meindl, T. (2010). Effects of aging on default mode network activity in resting state fMRI: Does the method of analysis matter? *Neuroimage, 51*, 280–287.

Koch, W., Teipel, S., Mueller, S., Benninghoff, J., Wagner, M., Bokde, A. L., … Meindl, T. (2012). Diagnostic power of default mode network resting state fMRI in the detection of Alzheimers disease. *Neurobiology of Aging*, *33*(3), 466–478. doi: 10.1016/j.neurobiolaging.2010.04.013

Koelsch, S. & Skouras, S. (2014). Functional centrality of amygdala, striatum and hypothalamus in a "small-world" network underlying joy: an fMRI study with music. *Hum Brain Mapp, 35*, 3485–98.

Koelsch, S., Skouras, S., & Lohmann, G. (2018). The auditory cortex hosts network nodes influential for emotion processing: An fMRI study on music-evoked fear and joy. *Plos One, 13*(1). doi:10.1371/journal.pone.0190057

Kübler, A., Dixon, V., & Garavan, H. (2006). Automaticity and Reestablishment of Executive Control—An fMRI Study. *Journal of Cognitive Neuroscience, 18*(8), 1331-1342. doi:10.1162/jocn.2006.18.8.1331

Laird, A. R., Fox, P. M., Eickhoff, S. B., Turner, J. A., Ray, K. L., Mckay, D. R., . . . Fox, P. T. (2011). Behavioral Interpretations of Intrinsic Connectivity Networks. *Journal of Cognitive Neuroscience, 23*(12), 4022-4037. doi:10.1162/jocn_a_00077

Lee, M. H., Hacker, C. D., Snyder, A. Z., Corbetta, M., Zhang, D., Leuthardt, E. C., & Shimony, J. S. (2012). Clustering of Resting State Networks. *PLoS ONE*, *7*(7). doi: 10.1371/journal.pone.0040370

Leech, R., Kamourieh, S., Beckmann, C. F., & Sharp, D. J. (2011). Fractionating the Default

Mode Network: Distinct Contributions of the Ventral and Dorsal Posterior Cingulate Cortex to Cognitive Control. *Journal of Neuroscience, 31*(9), 3217-3224. doi:10.1523/jneurosci.5626-10.2011

Lehmann, M., Madison, C., Ghosh, P. M., Miller, Z. A., Greicius, M. D., Kramer, J. H., . . . Rabinovici, G. D. (2015). Loss of functional connectivity is greater outside the default mode network in nonfamilial early-onset Alzheimer's disease variants. *Neurobiology of Aging, 36*(10), 2678-2686. doi:10.1016/j.neurobiolaging.2015.06.029

Li, K., Guo, L., Nie, J., Li, G., & Liu, T. (2009). Review of methods for functional brain connectivity detection using fMRI. *Computerized Medical Imaging and Graphics, 33*(2), 131-139. doi:10.1016/j.compmedimag.2008.10.011

Liu, Z., Zhang, Y., Yan, H., Bai, L., Dai, R., Wei, W., … Tian, J. (2012). Altered topological patterns of brain networks in mild cognitive impairment and Alzheimers disease: A resting-state fMRI study. *Psychiatry Research: Neuroimaging*, *202*(2), 118–125. doi: 10.1016/j.pscychresns.2012.03.002

Lohmann, G., Müller, K., Bosch, V., Mentzel, H., Hessler, S., et al. (2001). LIPSIA - a new software system for the evaluation of functional magnetic resonance images of the human brain. *Comp Med Imaging and Graphics, 25*, 449–457.

Lohmann, G., Margulies, D.S., Horstmann, A., Pleger, B., Lepsien, J., Goldhahn, D., Schloegl, H., …, Turner, R. (2010). Eigenvector centrality mapping for analyzing connectivity patterns in fMRI data of the human brain. *PloS One, 5*, e10232.

Long, X.-Y., Zuo, X.-N., Kiviniemi, V., Yang, Y., Zou, Q.-H., Zhu, C.-Z., … Zang, Y.-F. (2008). Default mode network as revealed with multiple methods for resting-state functional MRI analysis. *Journal of Neuroscience Methods*, *171*, 349–355. doi: 10.1016/j.jneumeth.2008.03.021

Luo, Z., Zeng, L., Qin, J., Hou, C., Shen, H., & Hu, D. (2019). Functional Parcellation of

Human Brain Precuneus Using Density-Based Clustering. *Cerebral Cortex, 30*(1), 269-282. doi:10.1093/cercor/bhz086

Marcus, D. S., Harms, M. P., Snyder, A. Z., Jenkinson, M., Wilson, J. A., Glasser, M. F., . . . Essen, D. C. (2013). Human Connectome Project informatics: Quality control, database services, and data visualization. *NeuroImage, 80*, 202-219. doi:10.1016/j.neuroimage.2013.05.077

Marek, S., & Dosenbach, N. (2018). The frontoparietal network: function, electrophysiology, and importance of individual precision mapping. *Dialogues in clinical neuroscience*, *20*(2), 133–140.

Margulies, D. S., Vincent, J. L., Kelly, C., Lohmann, G., Uddin, L. Q., Biswal, B. B., . . . Petrides, M. (2009). Precuneus shares intrinsic functional architecture in humans and monkeys. *Proceedings of the National Academy of Sciences, 106*(47), 20069-20074. doi:10.1073/pnas.0905314106

Markett, S., Montag, C., Heeren, B., Saryiska, R., Lachmann, B., Weber, B., & Reuter, M. (2015). Voxelwise eigenvector centrality mapping of the human functional connectome reveals an influence of the catechol-O-methyltransferase val158met polymorphism on the default mode and somatomotor network. *Brain Structure and Function*, *221*, 2755–2765. doi: 10.1007/s00429-015-1069-9

Mars, R. B., Sallet, J., Schuffelgen, U., Jbabdi, S., Toni, I., & Rushworth, M. F. (2011). Connectivity-Based Subdivisions of the Human Right "Temporoparietal Junction Area": Evidence for Different Areas Participating in Different Cortical Networks. *Cerebral Cortex, 22*(8), 1894-1903. doi:10.1093/cercor/bhr268

Mayes, S. D., Calhoun, S. L., Mayes, R. D., & Molitoris, S. (2012). Autism and ADHD: Overlapping and discriminating symptoms. *Research in Autism Spectrum Disorders, 6*(1), 277-285. doi:10.1016/j.rasd.2011.05.009

Mayhew, S. D., Ostwald, D., Porcaro, C., & Bagshaw, A. P. (2013). Spontaneous EEG alpha

oscillation interacts with positive and negative BOLD responses in the visual–auditory cortices and default-mode network. *NeuroImage, 76*, 362-372. doi:10.1016/j.neuroimage.2013.02.070

McKeown, M.J., Makeig, S., Brown, G.G., Jung, T.-P., Kindermann, S.S., Bell, A.J., & Sejnowski, T.J. (1998). Analysis of fMRI data by blind separation into independent spatial components. *Hum. Brain Mapp., 6*, 160–188.

Meda, S. A., Gill, A., Stevens, M. C., Lorenzoni, R. P., Glahn, D. C., Calhoun, V. D., . . . Pearlson, G. D. (2012). Differences in Resting-State Functional Magnetic Resonance Imaging Functional Network Connectivity Between Schizophrenia and Psychotic Bipolar Probands and Their Unaffected First-Degree Relatives. *Biological Psychiatry, 71*(10), 881-889. doi:10.1016/j.biopsych.2012.01.025

Mennes, M., Potler, N. V., Kelly, C., Martino, A. D., Castellanos, F. X., & Milham, M. P. (2012). Resting State Functional Connectivity Correlates of Inhibitory Control in Children with Attention-Deficit/Hyperactivity Disorder. Frontiers in Psychiatry, 2. doi:10.3389/fpsyt.2011.00083

Menon, V. (2011). Large-scale brain networks and psychopathology: A unifying triple network model. *Trends in Cognitive Sciences, 15*(10), 483-506. doi:10.1016/j.tics.2011.08.003

Meunier, D., Lambiotte, R., Fornito, A., Ersche, K. D., & Bullmore, E. T. (2009). Hierarchical modularity in human brain functional networks. *Frontiers in Neuroinformatics, 3*. doi:10.3389/neuro.11.037.2009

Mo, J., Liu, Y., Huang, H., & Ding, M. (2013). Coupling between visual alpha oscillations and default mode activity. *NeuroImage, 68*, 112-118. doi:10.1016/j.neuroimage.2012.11.058

Moeller, S., Yacoub, E., Olman, C.A., Auerbach, E., Strupp, J., Harel, N., & Ugurbil, K.

(2010). Multiband multislice GE-EPI at 7 tesla, with 16-fold acceleration using partial parallel imaging with application to high spatial and temporal whole-brain fMRI. *Magn Reson Med. 63*, 1144-1153.

Moosmann, M., Ritter, P., Krastel, I., Brink, A., Thees, S., Blankenburg, F., . . . Villringer, A. (2003). Correlates of alpha rhythm in functional magnetic resonance imaging and near infrared spectroscopy. *NeuroImage, 20*(1), 145-158. doi:10.1016/s1053-8119(03)00344-6

Najt, P., Perez, J., Sanches, M., Peluso, M.A.M, Glahn, D., & Soares, J.C. (2007). Impulsivity and bipolar disorder. *European Neuropsychopharmacology, 17*, 313-320. doi: 10.1016/j.euroneuro.2006.10.002

Nir, Y., Hasson, U., Levy, I., Yeshurun, Y., & Malach, R. (2006). Widespread functional connectivity and fMRI fluctuations in human visual cortex in the absence of visual stimulation. *NeuroImage, 30*(4), 1313-1324. doi:10.1016/j.neuroimage.2005.11.018

O'Brien, R. G. & Kaiser, M. K. (1985). The MANOVA approach for analyzing repeated measures designs: An extensive primer. *Psychological Bulletin*, *97*, 316–333. doi: 10.1037/0033-2909.97.2.316

Osipova, D., Ahveninen, J., Jensen, O., Ylikoski, A., & Pekkonen, E. (2005). Altered generation of spontaneous oscillations in Alzheimer's disease. *NeuroImage, 27*(4), 835-841. doi:10.1016/j.neuroimage.2005.05.011

Ouzir, M. (2013). Impulsivity in schizophrenia: A comprehensive update. *Aggression and Violent Behavior, 18*(2), 247-254. doi:10.1016/j.avb.2012.11.014

Palva, S., & Palva, J. M. (2007). New vistas for α-frequency band oscillations. *Trends in Neurosciences, 30*(4), 150-158. doi:10.1016/j.tins.2007.02.001

Power, J.D., Cohen, A.L., Nelson, S.M., Wig, G.S., Barnes, K.A., Church, J.A., Vogel, A.C., … Petersen, S.E. (2011). Functional Network Organization of the Human Brain. *Neuron, 72*, 665-678. doi: 10.1016/j.neuron.2011.09.006

Pruim, R. H., Mennes, M., Buitelaar, J. K., & Beckmann, C. F. (2015). Evaluation of ICA-AROMA and alternative strategies for motion artifact removal in resting state fMRI. *NeuroImage*, *112*, 278–287. doi: 10.1016/j.neuroimage.2015.02.063

Raichle, M.E. (2015). The Brain's default network. *Annual Review of Neuroscience, 38*, 433-47.

Raichle, M.E., MacLeod, A.M., Snyder, A.Z., Powers, W.J., Gusnard, D.A., & Shulman, G.L. (2001). A default mode of brain function. *PNAS, 98*, 676–82.

Ren, Y., Guo, L., & Guo, C. C. (2019). A connectivity-based parcellation improved functional representation of the human cerebellum. *Scientific Reports, 9*(1). doi:10.1038/s41598-019-45670-6

Rochat, L., Delbeuck, X., Billieux, J., D'acremont, M., Linden, A. J., & Linden, M. V. (2008). Assessing Impulsivity Changes in Alzheimer Disease. *Alzheimer Disease & Associated Disorders, 22*(3), 278-283. doi:10.1097/wad.0b013e318166d692

Sadaghiani, S., & D'Esposito, M. (2014). Functional Characterization of the Cingulo-Opercular Network in the Maintenance of Tonic Alertness. *Cerebral Cortex*, *25*(9), 2763–2773. doi: 10.1093/cercor/bhu072

Sanz-Arigita, E. J., Schoonheim, M. M., Damoiseaux, J. S., Rombouts, S. A., Maris, E., Barkhof, F., . . . Stam, C. J. (2010). Loss of 'Small-World' Networks in Alzheimer's Disease: Graph Analysis of fMRI Resting-State Functional Connectivity. *PLoS ONE, 5*(11). doi:10.1371/journal.pone.0013788

Scheeringa, R., Petersson, K. M., Kleinschmidt, A., Jensen, O., & Bastiaansen, M. C. (2012). EEG Alpha Power Modulation of fMRI Resting-State Connectivity. *Brain Connectivity, 2*(5), 254-264. doi:10.1089/brain.2012.0088

Seeley, W. W., Menon, V., Schatzberg, A. F., Keller, J., Glover, G. H., Kenna, H., . . .

Greicius, M. D. (2007). Dissociable Intrinsic Connectivity Networks for Salience Processing and Executive Control. *Journal of Neuroscience, 27*(9), 2349-2356. doi:10.1523/jneurosci.5587-06.2007

Shulman, G. L., Fiez, J. A., Corbetta, M., Buckner, R. L., Miezin, F. M., Raichle, M. E., & Petersen, S. E. (1997). Common Blood Flow Changes across Visual Tasks: II. Decreases in Cerebral Cortex. *Journal of Cognitive Neuroscience, 9*(5), 648-663. doi:10.1162/jocn.1997.9.5.648

Skouras, S., Falcon, C., Tucholka, A., Rami, L., Sanchez-Valle, R., Lladó, A., . . . Molinuevo, J. L. (2019). Mechanisms of functional compensation, delineated by eigenvector centrality mapping, across the pathophysiological continuum of Alzheimer's disease. *NeuroImage: Clinical, 22*, 101777. doi:10.1016/j.nicl.2019.101777

Skouras, S., Torner, J., Andersson, P., Koush, Y., Falcon, C., Minguillon, C., . . . Vilor-Tejedor, N. (2020). Earliest amyloid and tau deposition modulate the influence of limbic networks during closed-loop hippocampal downregulation. *Brain, 143*(3), 976-992. doi:10.1093/brain/awaa011

Smallwood, J., Brown, K., Baird, B., & Schooler, J. W. (2012). Cooperation between the default mode network and the frontal–parietal network in the production of an internal train of thought. *Brain Research, 1428*, 60-70. doi:10.1016/j.brainres.2011.03.072

Smith, S. M., Fox, P. T., Miller, K. L., Glahn, D. C., Fox, P. M., Mackay, C. E., . . . Beckmann, C. F. (2009). Correspondence of the brain's functional architecture during activation and rest. *Proceedings of the National Academy of Sciences, 106*(31), 13040-13045. doi:10.1073/pnas.0905267106

Smith, S.M., Andersson, J., Auerbach, E.J., Beckmann, C.F., Bijsterbosch, J., Douaud, G., Duff, E., … ,Glasser, M.F., for the WU-Minn HCP Consortium. (2013). Resting-state fMRI in the Human Connectome Project. *NeuroImage, 80,* 144–168.

Smith, S., & Nichols, T. (2009). Threshold-free cluster enhancement: Addressing problems of

smoothing, threshold dependence and localisation in cluster inference. *NeuroImage, 44*(1), 83-98. doi:10.1016/j.neuroimage.2008.03.061

Soddu, A., Vanhaudenhuyse, A., Bahri, M. A., Bruno, M., Boly, M., Demertzi, A., . . . Noirhomme, Q. (2011). Identifying the default-mode component in spatial IC analyses of patients with disorders of consciousness. *Human Brain Mapping, 33*(4), 778-796. doi:10.1002/hbm.21249

Sporns, O. (2013). Network attributes for segregation and integration in the human brain. *Current Opinion in Neurobiology*, *23*(2), 162–171. doi: 10.1016/j.conb.2012.11.015

Spreng, R. N., Stevens, W. D., Chamberlain, J. P., Gilmore, A. W., & Schacter, D. L. (2010). Default network activity, coupled with the frontoparietal control network, supports goal-directed cognition. *NeuroImage, 53*(1), 303-317. doi:10.1016/j.neuroimage.2010.06.016

Sridharan, D., Levitin, D. J., & Menon, V. (2008). A critical role for the right fronto-insular cortex in switching between central-executive and default-mode networks. *Proceedings of the National Academy of Sciences, 105*(34), 12569-12574. doi:10.1073/pnas.0800005105

Tagliazucchi, E., Wegner, F. V., Morzelewski, A., Brodbeck, V., & Laufs, H. (2012). Dynamic BOLD functional connectivity in humans and its electrophysiological correlates. *Frontiers in Human Neuroscience, 6*. doi:10.3389/fnhum.2012.00339

Taruffi, L., Pehrs, C., Skouras, S., & Koelsch, S. (2017). Effects of Sad and Happy Music on Mind-Wandering and the Default Mode Network. *Scientific Reports*, *7*(1). doi: 10.1038/s41598-017-14849-0

Tian, L., Jiang, T., Wang, Y., Zang, Y., He, Y., Liang, M., . . . Zhuo, Y. (2006). Altered resting-state functional connectivity patterns of anterior cingulate cortex in adolescents with attention deficit hyperactivity disorder. *Neuroscience Letters, 400*(1-2), 39-43. doi:10.1016/j.neulet.2006.02.022

Tian, L., Ren, J., & Zang, Y. (2012). Regional homogeneity of resting state fMRI signals predicts Stop signal task performance. *NeuroImage, 60*(1), 539-544. doi:10.1016/j.neuroimage.2011.11.098

Tomasi, D., & Volkow, N. D. (2011a). Functional connectivity hubs in the human brain. *NeuroImage*, *57*(3), 908–917. doi: 10.1016/j.neuroimage.2011.05.024

Tomasi, D., & Volkow, N. D. (2011b). Association between Functional Connectivity Hubs and Brain Networks. *Cerebral Cortex, 21*(9), 2003-2013. doi:10.1093/cercor/bhq268

Vaidya, C. J., & Gordon, E. M. (2013). Phenotypic Variability in Resting-State Functional Connectivity: Current Status. *Brain Connectivity, 3*(2), 99-120. doi:10.1089/brain.2012.0110

Van den Heuvel, M. P., Mandl, R. C., Kahn, R. S., & Pol, H. E. (2009). Functionally linked resting-state networks reflect the underlying structural connectivity architecture of the human brain. *Human Brain Mapping, 30*(10), 3127-3141. doi:10.1002/hbm.20737

Van den Heuvel, M. P., & Sporns, O. (2011). Rich-Club Organization of the Human Connectome. *Journal of Neuroscience, 31*(44), 15775-15786. doi:10.1523/jneurosci.3539-11.2011

Van Essen, D. V., Ugurbil, K., Auerbach, E., Barch, D., Behrens, T., Bucholz, R., . . . Yacoub, E. (2012). The Human Connectome Project: A data acquisition perspective. *NeuroImage, 62*(4), 2222-2231. doi:10.1016/j.neuroimage.2012.02.018

Van Essen, D. C., Smith, S. M., Barch, D. M., Behrens, T. E., Yacoub, E., & Ugurbil, K. (2013). The WU-Minn Human Connectome Project: An overview. *NeuroImage, 80*, 62-79. doi:10.1016/j.neuroimage.2013.05.041

Vincent, J. L., Kahn, I., Snyder, A. Z., Raichle, M. E., & Buckner, R. L. (2008). Evidence for a Frontoparietal Control System Revealed by Intrinsic Functional Connectivity. *Journal of Neurophysiology, 100*(6), 3328-3342. doi:10.1152/jn.90355.2008

Wang, K., Jiang, T., Yu, C., Tian, L., Li, J., Liu, Y., . . . Li, K. (2008). Spontaneous Activity

Associated with Primary Visual Cortex: A Resting-State fMRI Study. *Cerebral Cortex, 18*(3), 697-704. doi:10.1093/cercor/bhm105

Wang, L., Zhu, C., He, Y., Zang, Y., Cao, Q., Zhang, H., . . . Wang, Y. (2009). Altered small-world brain functional networks in children with attention-deficit/hyperactivity disorder. *Human Brain Mapping, 30*(2), 638-649. doi:10.1002/hbm.20530

Wang, J., Barstein, J., Ethridge, L. E., Mosconi, M. W., Takarae, Y., & Sweeney, J. A. (2013). Resting state EEG abnormalities in autism spectrum disorders. *Journal of Neurodevelopmental Disorders, 5*(1). doi:10.1186/1866-1955-5-24

Weiler, M., Teixeira, C. V., Nogueira, M. H., Campos, B. M., Damasceno, B. P., Cendes, F., & Balthazar, M. L. (2014). Differences and the Relationship in Default Mode Network Intrinsic Activity and Functional Connectivity in Mild Alzheimer's Disease and Amnestic Mild Cognitive Impairment. *Brain Connectivity, 4*(8), 567-574. doi:10.1089/brain.2014.0234

Wink, A. M., Munck, J. C. D., Werf, Y. D. V. D., Heuvel, O. A. V. D., & Barkhof, F. (2012). Fast Eigenvector Centrality Mapping of Voxel-Wise Connectivity in Functional Magnetic Resonance Imaging: Implementation, Validation, and Interpretation. *Brain Connectivity*, *2*(5), 265–274. doi: 10.1089/brain.2012.0087

Winstanley, C. A., Eagle, D. M., & Robbins, T. W. (2006). Behavioral models of impulsivity in relation to ADHD: Translation between clinical and preclinical studies. *Clinical Psychology Review, 26*(4), 379-395. doi:10.1016/j.cpr.2006.01.001

Woltering, S., Jung, J., Liu, Z., & Tannock, R. (2012). Resting state EEG oscillatory power differences in ADHD college students and their peers. *Behavioral and Brain Functions, 8*(1), 60. doi:10.1186/1744-9081-8-60

Xia, M., Wang, J., & He, Y. (2013). BrainNet Viewer: A Network Visualization Tool for Human Brain Connectomics. PLoS ONE 8: e68910.

Xie, C., Li, S., Shao, Y., Fu, L., Goveas, J., Ye, E., . . . Zhang, Z. (2011). Identification of

hyperactive intrinsic amygdala network connectivity associated with impulsivity in abstinent heroin addicts. *Behavioural Brain Research, 216*(2), 639-646. doi:10.1016/j.bbr.2010.09.004

Xu, J., Moeller, S., Strupp, J., Auerbach, E., Feinberg, DA., Ugurbil, K., & Yacoub, E. (2012). Highly accelerated whole brain imaging using aligned-blipped-controlled-aliasing multiband EPI. *Proc. Int. Soc. Mag. Reson. Med. 20*, 2306.

Yeo, B. T., Krienen, F. M., Sepulcre, J., Sabuncu, M. R., Lashkari, D., Hollinshead, M., . . . Buckner, R. L. (2011). The organization of the human cerebral cortex estimated by intrinsic functional connectivity. *Journal of Neurophysiology, 106*(3), 1125-1165. doi:10.1152/jn.00338.2011

Zhang, S., & Li, C. R. (2012). Functional connectivity mapping of the human precuneus by resting state fMRI. *NeuroImage, 59*(4), 3548-3562. doi:10.1016/j.neuroimage.2011.11.023

Zhang, Z., Zhang, D., Wang, Z., Li, J., Lin, Y., Chang, S., . . . Liu, M. (2018). Intrinsic Neural Linkage between Primary Visual Area and Default Mode Network in Human Brain: Evidence from Visual Mental Imagery. *Neuroscience, 379*, 13-21. doi:10.1016/j.neuroscience.2018.02.033

Zuo, X.N., Kelly, C., Adelstein, J.S., Klein, D.F., Castellanos, F.X., & Milham, M.P. (2010). Reliable intrinsic connectivity networks: test-retest evaluation using ICA and dual regression approach. *Neuroimage, 49*, 2163-2177.

Zuo, X.-N., Ehmke, R., Mennes, M., Imperati, D., Castellanos, F. X., Sporns, O., & Milham, M. P. (2012). Network Centrality in the Human Functional Connectome. *Cerebral Cortex*, *22*(8), 1862–1875. doi: 10.1093/cercor/bhr269